

THE UNIVERSITY OF CALGARY

GPS/INS Integration for Airborne Applications

by

Huangqi Sun

A THESIS

SUBMITTED TO THE FACULTY OF GRADUATE STUDIES
IN PARTIAL FULFILLMENT OF THE REQUIREMENTS FOR THE
DEGREE OF MASTER OF SCIENCE

DEPARTMENT OF GEOMATICS ENGINEERING

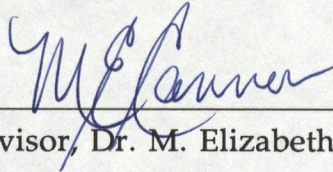
CALGARY, ALBERTA

SEPTEMBER, 1994

© Huangqi Sun 1994

THE UNIVERSITY OF CALGARY
FACULTY OF GRADUATE STUDIES

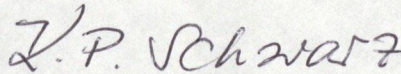
The undersigned certify that they have read, and recommend to the Faculty of Graduate Studies for acceptance, a thesis entitled "GPS/INS Integration for Airborne Applications" submitted by Huangqi Sun in partial fulfillment of the requirements for the degree of Master of Science.



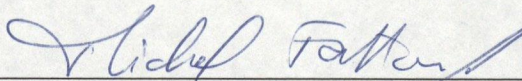
Supervisor, Dr. M. Elizabeth Cannon
Department of Geomatics Engineering



Dr. Gérard Lachapelle
Department of Geomatics Engineering



Dr. Klaus-Peter Schwarz
Department of Geomatics Engineering



Dr. Michel Fattouche
Department of Electrical and Computer Engineering

Date: October 19, 1994

ABSTRACT

The integration of DGPS with an INS is investigated for position, velocity and attitude determination in airborne applications. Fundamental aspects of GPS and INS are introduced. A centralized Kalman filter approach is used to incorporate DGPS measurements with the INS position, velocity and attitude. The errors during barometric aiding of the vertical channel are analyzed. Flight tests are used to demonstrate that the integrated system can provide aircraft positions at the centimetre level. In order to relieve the GPS signal shading problem, a strategy of integrating INS with multiple GPS antennas is studied. Three pairs of independent double difference carrier phase can keep INS updated. The attitude from a non-dedicated multi-antenna GPS attitude system is evaluated and the accuracy is in a few arcmins level after applying a aircraft wing flexure model. The wing flexure is determined and the magnitude is about 12 centimetres for the Twin Otter aircraft.

ACKNOWLEDGMENTS

I would like to express my deep gratitude to my supervisor, Dr. M. Elizabeth Cannon for her continuous support and encouragement throughout the course of my graduate studies. Her advice and guidance were essential for the completion of this thesis. Special thanks go to Dr. Gérard Lachapelle for his support and encouragement during the period of my graduate studies.

Mr. Todd Owen is thanked for his support and many discussions related to this research. He and Messrs. Mark Meindl, Doug Roberts also performed flight tests used in this research.

Dr. Klaus-Peter Schwarz is thanked for clarifying many concepts about INS. Mr. Gang Lu is thanked for his willingness to share his softwares and his experience in GPS data processing and software development. Thanks also go to Dr. M. Wei and Messrs. Gengsheng Zhang, Ziwen Liu and John Q. Zhang for their help in solving INS problems. Many of the fellow graduate students, Messrs. Dingsheng Chen, Jing Shi, Zoufa Li, John Brown, Doug Roberts, Richard Klukas are thanked for their discussions. All of them made my graduate studies enjoyable.

This work was supported by a contract with Sandia National Laboratories. Contribution of a Graduate Research Assistantship from The University of Calgary is also acknowledged.

Finally thanks go to my wife, Lin Feng for her patience, understanding and love during my graduate studies.

TABLE OF CONTENTS

APPROVAL PAGE.....	ii
ABSTRACT.....	iii
ACKNOWLEDGMENTS.....	iv
TABLE OF CONTENTS.....	v
LIST OF TABLES.....	vii
LIST OF FIGURES.....	viii
NOTATION	xii

CHAPTER	Page
1 INTRODUCTION	1
1.1 Background and Objective.....	1
1.2 Thesis Outline	6
2 GLOBAL POSITIONING SYSTEM.....	7
2.1 General Description.....	7
2.2 The GPS Positioning Principle.....	9
2.3 Differential Observations and Errors.....	11
3 INERTIAL NAVIGATION SYSTEM.....	14
3.1 INS Hardware Configuration.....	14
3.2 INS Mechanization	15
3.2.1 Mechanization of the Local Level System.....	15
3.2.2 Mechanization of the Strapdown System	17

3.3	Vertical Channel Aiding	18
3.4	INS Initial Alignment	21
3.4.1	Coarse Alignment.....	21
3.4.2	Fine Alignment.....	23
3.4.3	In-Flight Alignment.....	24
4	METHODOLOGY	25
4.1	Kalman Filter Algorithm.....	25
4.2	INS Error Modeling.....	28
4.3	Vertical Channel Aiding.....	31
4.4	GPS/INS Integration	32
4.4.1	Cycle Slip Detection and Correction Algorithm	35
4.5	GPS/INS Integration Software.....	38
5	TESTING AND RESULTS	41
5.1	Hardware Description.....	41
5.2	Test Description.....	44
5.3	Attitude Comparison Between Multi-GPS System and INS.....	47
5.4	Position and Attitude Results of GPS/INS Integration.....	61
5.4.1	Results of the Strapdown Configuration.....	62
5.4.2	Results of the Gimbal Configuration	72
5.5	Integration of INS with Multi-GPS Antennas	76
6	SUMMARY, CONCLUSIONS AND RECOMMENDATIONS	89
6.1	Conclusions.....	90
6.2	Recommendations	91
	REFERENCES	93

LIST OF TABLES

No.		Page
5.1	Distances Between the Four Antennas and the IMU	45
5.2	Coordinates of the Four Antennas in the Antenna Platform Frame.....	49
5.3	RMS of the Differences Between Attitude from a Multi-Antenna GPS System and an INS.....	59
5.4	GPS/INS Kalman Filter Spectral Densities.....	62
5.5	RMS of the Differences Between Aircraft Trajectories Computed from Two Ground Reference Stations.....	64
5.6	RMS of the Differences Between the GPS-only Positions and the GPS/INS Positions for the February 1 Test.....	67
5.7	GPS Antenna Coordinates in the IMU-Body Frame.....	77

LIST OF FIGURES

No.		Page
2.1	GPS Satellite Constellation.....	8
2.2	Absolute GPS Positioning.....	10
2.3	Double Differencing GPS Positioning	12
3.1	Wander Azimuth Mechanization for a Gimbal System.....	17
3.2	Wander Azimuth Mechanization for a Strapdown System.....	18
3.3	Vertical Channel Aiding Using Barometric Height.....	21
4.1	Concept of an Open-Loop GPS/INS Integration.....	33
4.2	GPS/INS Integration Scheme	34
4.3	The Cycle Slip Detection and Correction Scheme	36
4.4	GPS/INS Integration Software Flowchart.....	40
5.1	The DCH-16 Twin Otter Series 300.....	42
5.2	Layout of the GPS Antennas During the February Test.....	44
5.3	The Location of RLGA IMU	45
5.4	Satellites Observed at the Monitor Receiver During the February 1 Test.....	46
5.5	Definition of the Antenna Platform Frame.....	49
5.6	Aircraft Attitude During the February 4 Test.....	54
5.7	Aircraft Trajectory During the February 4 Test	55
5.8	PDOP and Number of Satellites Observed at Forward and Aft Antennas During the February 4 Test.....	56
5.9	PDOP and Number of Satellites Observed at Port and Starboard	

	Antennas During the February 4 Test.....	57
5.10	Roll, Pitch and Heading Differences Between Attitude From GPS Multiple Antenna System and INS Attitude For the Feb. 4 Test.....	58
5.11	Roll, Pitch and Heading Differences Between Attitude From a GPS Multi-Antenna System and an INS for the February Test When Using Wing Flexure Model.....	60
5.12	Wing Flexure of the Aircraft During the February 4	61
5.13	Aircraft Trajectory During the February 1 Test.....	63
5.14	Position Differences Between the GPS-Only Solution and the GPS/INS Integration Solution During the February 1 Test.....	65
5.15	Position Differences Between the GPS-Only Solution and the GPS/INS Integration Solution During Feb. 1 Test When Using the Barometric Error Model.....	66
5.16	GPS Versus the Barometric Height and GPS Versus the Initial Aircraft Height	67
5.17	Horizontal Velocity Errors Estimated from GPS/INS Integration For the February 1 Test.....	68
5.18	Vertical Velocity Error Estimated from the GPS/INS Integration for the February Test.....	69
5.19	Horizontal Attitude Errors Estimated from the GPS/INS Integration for the February 1 Test.....	70
5.20	Heading Error Estimated from the GPS/INS Integration for the February 1 Test.....	70
5.21	Horizontal Attitude Errors Estimated From the GPS/INS	

Integration for the February Test when Using the Barometric Error Mode.....	71
5.22 Heading Error Estimated From the GPS/INS Integration for the February Test When Using the Barometric Error Model.....	71
5.23 Aircraft Trajectory During the June 20 Test.....	73
5.24 Position Differences Between the GPS-Only Solution and the GPS/INS Integration Solution for the June 20 Test.....	74
5.25 Horizontal Velocity Errors Estimated from GPS/INS for the June 20 Test.....	74
5.26 Horizontal Attitude Errors Estimated From GPS/INS for the June 20 Test.....	75
5.27 Heading Error Estimated from GPS/INS for the June 20 Test	75
5.28 Aircraft Trajectory During the February 2 Test	78
5.29 Number of Satellites Observed at the Forward, Aft and Port Antennas During the February 2 Test	79
5.30 Aircraft Roll and Pitch During the February 2 Test.....	80
5.31 Integration Strategy of the INS with Multiple GPS Antennas	82
5.32 Position Differences Between the INS Integrated with the Forward Antenna Only Versus the Reference Trajectory	83
5.33 Longitude Differences Between the INS Without Update and the Reference Trajectory.....	84
5.34 Position Differences Between the INS Integrated with the Forward and Aft Antennas Versus the References Trajectory.....	85

5.35	Position Differences Between the INS Integrated with Three Pairs of Double Differences Carrier Phase Measurements Versus the Reference Trajectory.....	87
5.36	The Aircraft Speed During Taxing and Take-off During the February 2 Test.....	88

NOTATION

i) Conventions

- (a) Matrices are uppercase and bold
- (b) Vectors are lower case and bold
- (c) Rotation matrices between coordinate systems are defined by a subscript and a superscript denoting the two coordinate system, e.g. \mathbf{R}_w^b indicates a transformation from the wander frame (w) to the body frame (b). The angular rate vector \mathbf{w}_{ib}^b , represents the rotation of the body frame with respect to the inertial frame coordinated in the body frame.
- (d) The operators are defined as:
 - (+) Kalman update]
 - (-) Kalman Prediction
 - $\dot{}$ derivation with respect to time
 - \mathbf{A}^T matrix transpose
 - \mathbf{A}^{-1} matrix inverse
 - Δ single difference between receivers
 - δ correction to
 - $f()$ is a function of
 - \hat{x} estimated value
 - ∇ single difference between satellites

ii) Coordinate Systems

Body (b): A right-handed system which defines the frame in which the raw INS measurements are made.

origin: at the center of the IMU

x-axis: towards the right side of the IMU

y-axis: towards the output pins of the IMU

z-axis: upwards, perpendicular to the x-y plane

Earth (e): A right-handed system which is usually defined by the Conventional Terrestrial Frame (CTS) as following:

origin: at the center of mass of the earth

x-axis: towards the mean meridian of Greenwich

y-axis: 90 degrees east of the Greenwich meridian

z-axis mean rotation axis of the earth

Inertial (i) A operational inertial frame which is used as an approximation to the true inertial frame. It is defined as

origin: at the center of mass of the earth

x-axis: towards the mean vernal equinox

y-axis completes a right-handed system

z-axis mean rotation axis of the earth

Local-level (n) A right-handed system used for the trajectory computation. It is defined with respect to a best fitting ellipsoid with origin at the earth's center of mass.

origin: at the center of IMU

x-axis: towards ellipsoid east

y-axis towards ellipsoid north
z-axis upwards, along ellipsoid normal

Wander (w) A right-handed system in which the INS computations are made. It is similar to the local-level frame except for a rotation in the x-y plane.

origin: at the center of the IMU
x-axis: rotated from the east towards the north on the level plane by an wander angle, α which is selected to be equal to the meridian convergence from the point of alignment
y-axis: orthogonal to the x-axis in the level plane
z-axis: upwards, along ellipsoidal normal

iii) Symbols

- A design matrix
- α wander angle; correlation length of gyro drift
- a acceleration vector
- β correlation length of accelerometer biases
- b accelerometer bias
- c speed of light
- C^e Kalman measurement noise covariance matrix
- C^w Kalman filter process noise covariance matrix
- C^x Kalman state vector covariance matrix
- d gyro drift
- dT receiver clock error

dt	satellite clock error
ε	measurement noise
Φ	carrier phase
F	dynamics matrix
Φ	Kalman filter transition matrix
φ	roll
f	carrier phase frequency, wing flexure
γ	normal gravity
h	geodetic height
I	identity matrix
K	Kalman gain matrix
K	damping ratio of vertical channel aiding
λ	geodetic longitude, carrier phase wavelength
l	vector of measurements
M	meridian radius of curvature
N	carrier phase ambiguity, prime vertical radius of curvature
P	covariance matrix
P	pseudorange
Q	spectral density matrix
θ	pitch
ρ	geometrical distance between receiver and satellite
R_E	earth radius
v	velocity vector
Ω	three parameter skew-symmetric matrix
ω	angular rate vector
w	process noise vector

x	kalman state vector
ψ	heading

iv) Acronyms

AS	Anti-spoofing
C/A Code	Clear/Acquisition code
GDOP	Geometric Dilution of Precision
GPS	Global Positioning System
INS	Inertial Navigation System
OTF	On the fly
P code	Precise code
PRN	Pseudo Random Noise
RMS	Root Mean Square
SA	Selective availability
SAR	Synthetic Aperture Radar
SNL	Sandia National Laboratories
ZUPT	Zero Velocity Update

CHAPTER 1

INTRODUCTION

1.1 Background and Objective

The Navstar Global Positioning System (GPS) is an advanced navigation system for the determination of position, velocity and time. Although originally designed for military use, GPS is also used extensively by the civilian community for land, shipborne and airborne applications, e.g. Mader (1986), Lachapelle et al. (1987), Cannon (1991). GPS can provide consistently accurate navigation parameters independent of time, location and weather. There are many new applications which are being investigated such as attitude determination with multiple GPS antennas, e.g. Schwarz et al. (1992), Cohen et al. (1993), Lu et al. (1993) and acceleration determination with GPS, e.g. Kleusberg (1990), Wei et al. (1992), Van Dierendonck et al. (1994).

Inertial Navigation Systems (INS) have been used for navigation since the 1960s. However they have only been used for surveying during the last three decades due to cost and accuracy limitations, e.g. Schwarz (1983), Wong (1988), Forsberg (1990). Although an INS tends to drift from truth with time, it can provide high short-term accuracy.

The integration of GPS and INS has been conceived since the emergence of GPS (Cox, 1978; Wong et al., 1983). Since GPS can provide consistent high accuracy position and velocity information, it can be used to update an INS to prevent drift. Some applications require very high data density but GPS at present can only provide relatively low data density trajectory information, typically less than 10 Hz. An INS can provide trajectory information of very high density, generally above 50 Hz. GPS is not a self-contained system since the receiver has to keep track of signals transmitted by the GPS satellites. These signals can be lost or shaded due to many reasons such as blockage of the signal path or receiver instability. In contrast, an INS is a self-contained system. GPS outages can be bridged by an INS using its short term stability, e.g. Lapucha (1990), Cannon (1991). The integration of GPS and INS can then provide uniform high accuracy and high data density.

Attitude is a required component for many applications, e.g. Bickel et al. (1993), Schwarz et al. (1993). An INS can provide accurate attitude information, however, it tends to drift in the long term. Using accurate GPS trajectory information to update the INS can partially control the drift of INS attitude. Due to the cost of an INS, GPS multiple antenna attitude systems have been under investigation for a few years, e.g. Purcell et al. (1989), Van Graas et al. (1991), Cohen et al. (1992), Schwarz et al. (1992), Lu et al. (1993). The accuracy achieved depends on the baseline length between the antennas in the direction of the attitude component (Lu et al., 1993). With a baseline of three metres, the achievable attitude accuracy is in the order of a few arcminutes. This baseline length limits the accuracy for many applications because of the difficulty in the

installation of antennas. The accuracy of attitude from a multiple GPS antenna system can fulfill the requirements for many applications where attitude parameters with an accuracy of few arcminutes are needed. However an INS is still the primary attitude determination system for the applications where attitude parameters better than 1 arcminute are required.

The integration of GPS and INS can be done in three different ways. The first one is the hardware integration (Cox, 1978; Hartman, 1988). GPS trajectory information can be used to update the INS and the velocity from INS can be used to assist GPS in tracking the satellites and narrow the GPS tracking bandwidth, thereby reducing the receiver noise. The second way is a closed loop software integration, e.g. Schwarz et al. (1984), Wong et al. (1988) where the GPS trajectory is used to update the INS output and the updated position, velocity and attitude enter the mechanization again, thus the prediction of the INS is based on more accurate values. The third way is an open loop software integration (Upadhyay et al., 1982; Sun et al., 1994). At present, since the real-time differential carrier phase position is still not operational due to the limit of techniques for carrier phase ambiguity resolution on the fly (OTF), the real-time integration of INS with GPS carrier phase is also not feasible. The gyro rate and accelerometer specific force have to be recorded during the data acquisition and then processed in post mission. A less accurate real-time solution is still needed in many applications (Owen et al., 1992), therefore the requirement of data logging speed is very high due to the large volume of data needed to be recorded. One trade-off is not to record the raw gyro and accelerometer output, but record the mechanization output position, velocity and attitude. The integration of GPS with INS is then

based on this output. The third method is used in the current investigation since the raw gyro rates and specific forces are not recorded for post-processing due to limitation in the data logging.

The vertical channel will diverge if only the INS is used (Siouris, 1993). Therefore, another source of height to constrain the INS is needed to keep the vertical channel stable. An inexpensive and convenient source is the barometer. The accuracy of height from a barometer depends on many aspects, such as the dynamics of the aircraft, wind speed and atmospheric parameters (Widnall, et al., 1980). Therefore, when the third integration method has to be used, the height component from the mechanization is influenced by barometric altitude errors. Therefore, modeling of barometric errors is needed in the integration. Another source of height is from real-time GPS point positioning or real-time differential pseudorange positioning (Cox, 1978; Owen et al., 1992). The same problem still exists in this mode. Because of the noise level in the code solution and the error from Selective Availability (SA), modeling of height errors is necessary in this research.

Many real-time and post-mission airborne GPS differential positioning tests have been conducted and centimetre-level or metre-level positions have been achieved for different applications, see e.g. Mader (1986), Keel et al. (1988). However, airborne GPS/INS tests have been limited, especially for high accuracy applications (Baustert et al., 1989; Cannon, 1991; Meyer-Hilberg et al., 1994). A number of GPS/INS flight tests have been conducted by Sandia National Laboratories (SNL) and The University of Calgary to evaluate the capability of

such a system to provide high accuracy position, velocity and attitude. The analysis of results are based on these tests.

The GPS antenna may be susceptible to shading, especially during the banking of an aircraft. However, the shading may not happen at another antenna located at a different position on the aircraft, therefore integration of an INS with multiple GPS antennas can relieve this problem (Sun, 1994). It can also improve the heading accuracy of the integrated system.

The objective of this research is to develop a post-mission GPS/INS integration system using the third method, namely the integration of GPS double difference carrier phase with the INS output position, velocity and attitude which is constrained by either barometric heights or GPS point positioning heights, to estimate the errors in position, velocity and attitude of the inertial measurement unit. One potential use of this system is to attach the IMU to a synthetic aperture radar (SAR) antenna to measure its position, velocity and attitude which can be used to correct the radar image (Fellerhoff et al., 1992). In SNL's interferometric SAR which can measure heights as well as horizontal positions, very accurate horizontal attitude parameters (especially the roll component) are required (Bickel et al., 1993). A roll error of 36 arcsecs will introduce a 1 metre error in height while a pitch error of 36 arcmins will introduce about 1 metre error in height.

1.2 Thesis Outline

The general concept of GPS and the principle of GPS positioning is introduced in Chapter 2. Error sources in the double difference carrier phase are also briefly reviewed. INS mechanization, vertical channel aiding as well as INS alignment methods are introduced in Chapter 3. In Chapter 4, the Kalman filter methodology is reviewed, the INS error modeling is described and the error modeling for the vertical channel is given. Cycle slip detection and correction schemes in a GPS-only system and GPS/INS integration system are discussed. The GPS/INS integration software is also outlined. In Chapter 5, the hardware for the flight test and the test description are introduced. Attitude parameters from the GPS multiple antenna system are compared with the INS attitude and then a wing flexure model is introduced for the aircraft. The estimated errors for position, velocity and attitude are given for both an INS strapdown configuration and a gimbal configuration. The integration of INS with multiple GPS antennas is introduced for more consistent and reliable trajectory results. In Chapter 6, conclusions are drawn and recommendations for future research are made.

CHAPTER 2

GLOBAL POSITIONING SYSTEM

This chapter gives a general introduction to GPS and the principle of GPS positioning. Error sources in the differential GPS observations are also outlined.

2.1 General Description

The Navstar Global Positioning System (GPS) is a satellite-based radio system designed for navigation. Using signals transmitted by the GPS satellites, it can provide three-dimensional position on a global basis, independent of weather conditions, virtually 24-hours per day. It is composed of a space segment, a control segment and a user segment.

The space segment is comprised of 24 GPS satellites orbiting about 20,200 km above the Earth's surface in six orbital planes (see Figure 2.1). There are four satellites evenly distributed in each plane. Each satellite transmits signals on two frequencies, one is called L1 at 1575.42 MHz and another one is called L2 at 1227.60 MHz. The L1 frequency is modulated by two pseudo random noise (PRN) codes, one is the coarse acquisition (C/A) code and the other is the precise (P) code. The L2 frequency is only modulated by the P code. The C/A code is

transmitted at 1.023 MHz and is repeated every 1 ms while the P code is transmitted at 10.23 MHz and is repeated every 267 days. The navigation message, which contains the GPS satellite orbit, clock and satellite health information is modulated on both frequencies. The receiver first tracks the C/A code and then tracks P code by a Hand Over Word (HOW) if the receiver has the P code capability (see Wells et al., 1987).

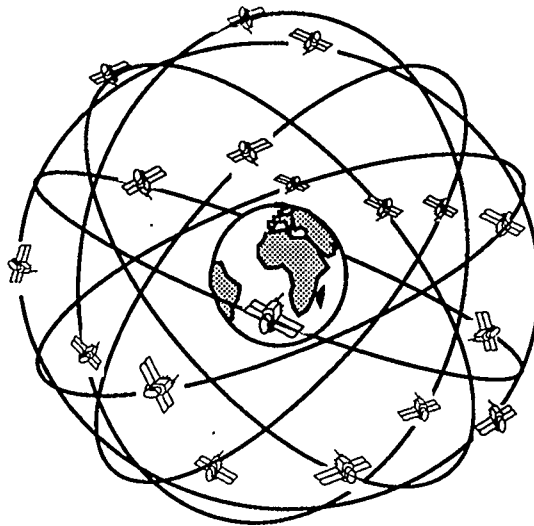


Figure 2.1
GPS Satellite Constellation

The GPS system was declared fully operational on February 17, 1994 when the 24-satellite constellation was complete. Therefore, at least 4 satellites can be tracked simultaneously everywhere on the earth. However, since Anti-spoofing (AS) is turned on, the P-code is converted to the Y-code which only authorized users have the key to access. Since receiver technology is developing quickly, many civilian receivers can still measure L2 pseudorange and carrier phase data through various codeless techniques. This will be further discussed below.

The control segment is composed of ground monitor stations that perform satellite tracking, orbit determination, uploading navigation messages to satellites and satellite control. The user segment consists of GPS receivers which receive the radio signals from the GPS satellites and compute the navigation solution from these signals.

Receiver technology has been developing rapidly. Due to the encryption of the P code, new C/A code receiver technology such as narrow correlator spacing which gives a ten centimetre code noise level (Van Dierendonck et al., 1992). New technology such as cross correlation has allowed a receiver to have the capability to measure a full wavelength L2 carrier phase without access to the Y-code (Meehan et al., 1987). Another codeless technology, i.e. the new P-W correlation technique, can allow a receiver not only to measure a full wavelength L2 carrier phase, but also to measure Y-code pseudoranges on both L1 and L2 frequencies (Ashjaee et al., 1992). This will benefit many GPS carrier phase applications assuming adequate signal strength can be observed. It will be further discussed below.

2.2 GPS Positioning Principle

There are two fundamental measurements from GPS, one is the pseudorange and the other is the carrier phase. The pseudorange is measured by comparing the code arriving from the satellite with a replica of the code generated in the receiver to determine the time shift to correlate the two signals. Carrier phase measurements are made on a beat phase which is formed by differencing the

incoming carrier phase with a reference signal generated by the receiver. Only the fractional part of one cycle can be measured accurately. The phase change is measured by the Doppler count which is the number of accumulated whole cycles. Therefore, the initial number of integer cycles in the carrier phase is unknown (Wells et al., 1987). This is the so-called carrier phase ambiguity.

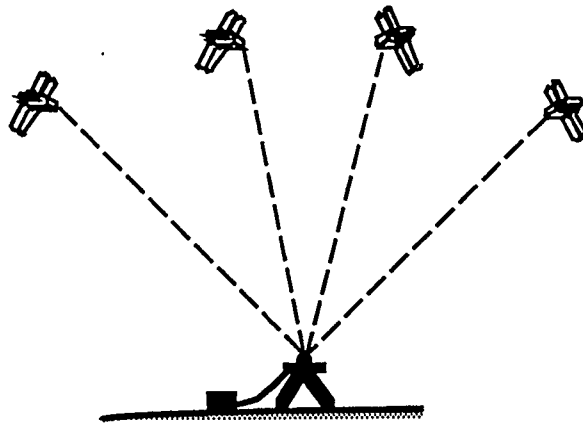


Figure 2.2
Absolute GPS Positioning

The principle of GPS positioning is shown in Figure 2.2. Four pseudoranges from four different satellites are used to solve the three position components and one receiver clock error. The pseudorange observation equation and the carrier phase observation equation can be expressed as

$$P = \rho + c(dt - dT) + d_{\text{ion}} + d_{\text{trop}} + d_{\rho} + \varepsilon_P \quad (2.1)$$

$$\Phi = \rho + c(dt - dT) + \lambda N - d_{\text{ion}} + d_{\text{trop}} + d_{\rho} + \varepsilon_{\Phi} \quad (2.2)$$

where P is the pseudorange observation (m)
 Φ is the carrier phase observation (m)

ρ	is the satellite-receiver range (m)
c	is the speed of light (m s^{-1})
dt	is the satellite clock error (s)
dT	is the receiver clock error (s)
λ	is the carrier phase wave length (m cycle^{-1})
N	is the carrier phase integer ambiguity (cycles)
d_{ion}	is the ionospheric correction (m)
d_{trop}	is the tropospheric correction (m)
d_{ρ}	is the orbital error (m)
and ε	is the measurement noise and multipath (m).

In Equations (2.1) and (2.2), $\rho = \|\mathbf{r}^s - \mathbf{r}_r\|$, where \mathbf{r}_r is the receiver position which must be determined and \mathbf{r}^s is the satellite coordinate vector which can be calculated using the broadcast satellite ephemerides.

Another fundamental observable is the phase rate, a measure of the induced Doppler effect due to satellite and vehicle motion. The observation equation of the phase rate can be formed by differentiating Equation (2.2).

2.3 Differential Observations and Errors

From Equations (2.1) and (2.2), it is known that there are several error sources in the pseudorange and carrier phase observations. These errors will significantly influence positioning results. In order to get high accuracy positions, differencing of the observations is used to eliminate most of the common errors. Between

receiver single differencing is done by subtracting the observation at the monitor station from that at the remote station for the same satellite. This difference can eliminate satellite-common errors including spatially correlated ionospheric error, tropospheric errors, orbital error and satellite clock error. Double difference observations can be made by further differencing two single differences across two satellites (see Figure 2.3). This difference will further eliminate the receiver clock error. The observation equations of the double difference pseudorange and carrier phase can be written as (Wells et al., 1987)

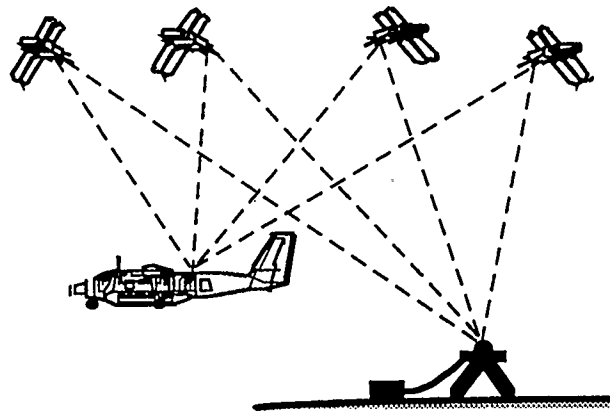


Figure 2.3

Double Differencing GPS Positioning

$$\Delta\nabla P = \Delta\nabla\rho + \Delta\nabla d_{\text{ion}} + \Delta\nabla d_{\text{trop}} + \Delta\nabla d_p + \varepsilon_{\Delta\nabla P} \quad (2.4)$$

$$\Delta\nabla\Phi = \Delta\nabla\rho + \lambda\Delta\nabla N - \Delta\nabla d_{\text{ion}} + \Delta\nabla d_{\text{trop}} + \Delta\nabla d_p + \varepsilon_{\Delta\nabla\Phi} \quad (2.5)$$

where $\Delta\nabla$ expresses the double difference of the corresponding value. The residual errors in the double difference observations are mostly due to the loss of spatial correlation as a function of distance and multipath. The common parts of the ionospheric and tropospheric error have been eliminated. Similarly the

common part of the orbital error has been removed. However, the noise is magnified. The multipath error cannot be eliminated since the multipath effect of the two receivers are generally not the same. Therefore the accuracy of double difference positioning largely depends on the distance between the ground receiver and the remote receiver and the level of multipath effect. If this distance is small, then the ionospheric and tropospheric errors are similar and the common parts of the errors can be eliminated. Most of the orbital error can also be eliminated. Multipath can be reduced by using an antenna with a choking ground plane. Also a new multipath reduction technique through signal processing, namely Multipath Elimination Technology (MET) was introduced (Townsend et al., 1994). A 30 to 70 percent reduction of multipath error effects in differential GPS pseudorange positioning was shown.

Another term in Equation (2.5) is ΔN . Theoretically it is an integer, however due to the influence of the ionospheric error, the tropospheric error and the multipath effect, it is difficult to obtain the correct integer especially when the baseline length is greater than 30 kilometres. Methods to obtain the correct integer have been an active research area during the last few years. Many different methods have been designed to search for this ambiguity within a short time and with high reliability, e.g. Hatch (1991), Lachapelle et al. (1993). A recent method is by Chen (1993) and Chen and Lachapelle (1994) where the success rate of the ambiguity search can reach ninety percent or higher while the number of epochs needed to get the ambiguity is below 1 minute for narrow correlator spacing single frequency receivers with good satellite geometry in land experiments.

CHAPTER 3

INERTIAL NAVIGATION SYSTEM

This chapter will introduce the INS hardware configuration, outline the principle of the inertial navigation systems (INS) and describe the INS mechanization. Vertical channel aiding as well as INS alignment methods will also be reviewed.

3.1 INS Hardware Configuration

There are three main types of INS, namely the space stabilized system, the local-level system and the strapdown system (Schmidt, 1978). In the space-stabilized system, the INS measurement frame does not rotate with respect to the inertial frame and the gyro does not experience any torque input. In the local-level system, the INS measurement frame does not rotate with respect to the local-level coordinate frame while a strapdown system is fixed to the vehicle body frame and the transformation matrix between the body frame and a computational reference frame is computed analytically. According to the torque applied to the vertical gyro, the local-level INS can be further subdivided into three types, namely the normal local level system, the free azimuth system and the rotating azimuth system (Britting, 1971). In the normal local-level system, the vertical channel is mechanized to allow the INS to align with the local north in

the azimuth direction. In the free azimuth system, the vertical gyro is uncommanded except by the compensation of the gyro nonorthogonality and noise, therefore the vertical gyro will always point to the same direction of the vertical gyro as that in the space-stabilized system. In the rotating azimuth system, the vertical gyro can be commanded to rotate at a relatively high speed.

The INS system used in this research can be configured as a strapdown or a local-level system. This system also has the ability to be rotated in the azimuth direction during the operation so that it can be pointed in different directions during a mission. Further information on the specific system used in this work is given in Section 5.1.

3.2 INS Mechanization

An INS can be mechanized in different coordinate systems, such as the earth-center-earth-fixed (ECEF) coordinate system (Wei et al., 1990), the local-level system or the wander azimuth system (Wong et al., 1983). However, since there are singularities at the poles for the ECEF system and the local-level frame, the wander azimuth system is commonly used.

3.2.1 Mechanization of the Local-Level System

As mentioned above, the mechanization of the local-level system is performed in the wander-azimuth frame in order to avoid singularities at the poles. The mechanization equations can be written in the following form (Britting, 1971)

$$\dot{\mathbf{r}}^n = \mathbf{D}^{-1}\mathbf{v}^n \quad (3.1)$$

$$\dot{\mathbf{v}}^n = \mathbf{R}_w^n \mathbf{f}^w - (\Omega_{en}^n + 2\Omega_{ie}^n) \mathbf{v}^n + \mathbf{g}^n \quad (3.2)$$

$$\dot{\alpha} = (\dot{\lambda} + \omega_{ie}) \sin\phi \quad (3.3)$$

where

$$\mathbf{D}^{-1} = \begin{pmatrix} 0 & 1/(M+h) & 0 \\ 1/(N+h)\cos\phi & 0 & 0 \\ 0 & 0 & 1 \end{pmatrix} \quad (3.4)$$

and

- \mathbf{r} is the position vector (m)
- \mathbf{v} is the velocity vector (m s^{-1})
- \mathbf{f} is the specific force vector (m s^{-2})
- \mathbf{R}_w^n is the transformation matrix from wander frame to local-level frame
- Ω is the angular velocity matrix (rad s^{-1})
- \mathbf{g} is the normal gravity vector (m s^{-2})
- α is the wander angle (rad)
- ϕ, λ, h are latitude (rad), longitude (rad) and height (m) respectively
- ω_{ie} is the angular velocity of earth rotation (rad s^{-1})
- M, N are the meridian and prime vertical radii of curvature, respectively (m).

The mechanization diagram is shown in Figure 3.1 (Schmidt, 1978). The gyro command which drives the gyro align to the wander-azimuth frame is ω_{iw}^w . It is expressed as (Wong, 1983)

$$\omega_{iw}^w = R_n^w \omega_{iw}^n R_w^n \quad (3.5)$$

where

$$\omega_{iw}^n = ((\dot{\lambda} + \omega_e) \cos \phi, -\dot{\phi}, 0)^T \quad (3.6)$$

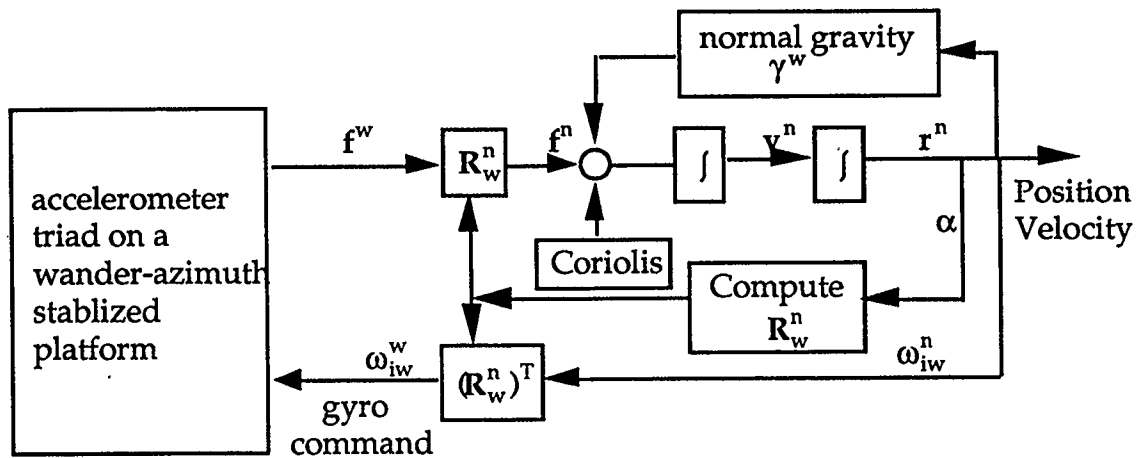


Figure 3.1

Wander Azimuth Mechanization for a Gimbal System (Schmidt, 1978)

3.2.2 Mechanization of the Strapdown System

For a strapdown system, the IMU is physically attached to the vehicle and it experiences the same movement. A computer-generated transformation matrix between the IMU body-frame and the desired output coordinate frame is used to transform the IMU acceleration and angular velocity, which is given in the body frame, to the desired output coordinate frame. The mechanization equations are

usually given in the local-level frame as Equations (3.7) to (3.9), but they are implemented in the wander azimuth frame. The mechanization diagram is illustrated in Figure 3.2 (Wong, 1988).

$$\dot{\mathbf{r}}^n = \mathbf{D}^{-1}\mathbf{v}^n \quad (3.7)$$

$$\dot{\mathbf{v}}^n = \mathbf{R}_b^n \mathbf{f}^b - (2\boldsymbol{\Omega}_{ie}^n + \boldsymbol{\Omega}_{en}^n)\mathbf{v}^n + \mathbf{g}^n \quad (3.8)$$

$$\dot{\mathbf{R}}_b^n = \mathbf{R}_b^n (\boldsymbol{\Omega}_{ib}^b - \boldsymbol{\Omega}_{in}^b) \quad (3.9)$$

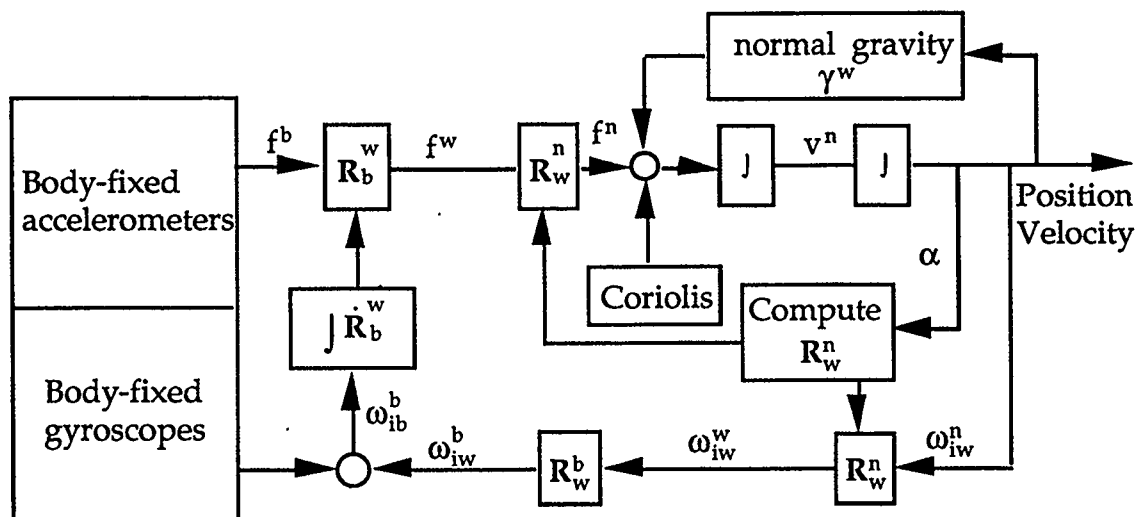


Figure 3.2

Wander-Azimuth Mechanization for a Strapdown System (Wong, 1988)

3.3 Vertical Channel Aiding

The vertical channel will diverge when only INS data is used, therefore other sources of altitude data are needed to constrain the height. A convenient source is barometric height. GPS height (from real-time point or differential positioning) is another source.

Since pressure and temperature change with height, it is possible to compute the height from these components using an empirical formula, e.g. the standard model (Siouris, 1992)

$$h_b = H_0 + \frac{T_0 \left[\frac{P}{P_0} - \frac{R \Gamma}{g_0 M} - 1 \right]}{\Gamma} \quad (3.10)$$

where

- h_b is the pressure altitude (m)
- H_0 is the height corresponding to the standard temperature (m)
- T is the measured temperature (K)
- T_0 is the standard temperature (K)
- P is the measured pressure (mb)
- P_0 is standard pressure (mb)
- R is the universal gas constant
- g_0 is gravity at the sea level ($m s^{-2}$)
- M is the mean molecular weight of the air
- and Γ is the lapse rate of temperature ($K m^{-1}$).

The pressure altitude can significantly differ from the true altitude. A magnitude of 5-10% of height is considered typical.

If the barometric height is used, a third-order loop is commonly used in order to obtain improved performance (Siouris, 1993). Figure 3.3 illustrates a standard

third-order vertical channel damping technique for mixed barometer and inertially derived height data. The mechanization of the baro-aiding equations is given in the wander-azimuth frame as following (Siouris, 1993).

$$\Delta h = h_i - h_b \quad (3.11)$$

$$\dot{a}_b = K_3 \Delta h \quad (3.12)$$

$$\dot{v}^u = f^u - (2\omega_{ie}^w + \omega_{ew}^w)v^e + (2\omega_{ie}^w + \omega_{iw}^w)v^n + \gamma^u + a_b + K_2 \Delta h \quad (3.13)$$

$$\dot{h} = v^u - K_1 \Delta h \quad (3.14)$$

where Δh is the difference between the barometric height, h_b , and the inertial height, h_i . It is the input of the loop. f^u is the vertical specific force, the second and third term in Equation (3.12) are Coriolis compensation, and γ^u is the normal gravity. One more variable, a_b , the barometric height acceleration, is added here to account for the barometric height characteristics. Three coefficients K_1 , K_2 and K_3 for the three loops are used to adjust the damping ratio. They are determined from specifications of the barometer, requirements of the aiding loop and the loop time constant of the system. The time constant is typically chosen to be 100-200 seconds.

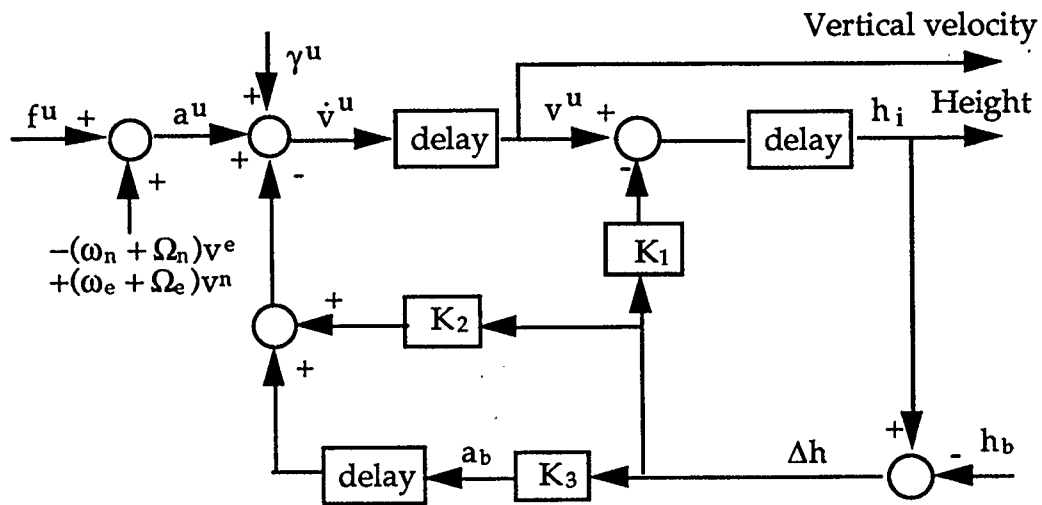


Figure 3.3

Vertical Channel Aiding Using Barometric Heights (Siouris, 1993)

3.4 Initial Alignment

Since an INS is a self-contained system, any initial errors will influence the results. Therefore, an initial alignment is a mandatory and important procedure. The alignment for the strapdown INS system consists of a coarse alignment and a fine alignment. An approximate attitude is determined during coarse alignment. This attitude is then used as a first-order approximation in the filter during the fine alignment stage.

3.4.1 Coarse Alignment

For a strapdown INS, the relation between the body frame and a desired output frame is computationally determined, therefore a coarse attitude must be input to the mechanization for the following computation. There are many ways to get

this attitude (Wong, 1988). The first method is to get it from other sources, such as a GPS multi-antenna attitude system or other low accuracy attitude sensors. The second way is from the memory-saved attitude from a previous mission. The attitude of the INS is saved after the aircraft landing. Assuming the aircraft has not moved, this stored attitude is used as an initial attitude for the alignment before the next mission. The third way is to perform a coarse alignment. Assuming the aircraft is stationary during alignment, only the earth's rotation and gravity are sensed by the INS. Therefore the roll, pitch and heading can be found. Since (e.g. Lapucha, 1990)

$$\omega_{ie}^w = \begin{pmatrix} \omega_{ie} \sin A \cos \phi \\ \omega_{ie} \cos A \cos \phi \\ \omega_{ie} \sin \phi \end{pmatrix} = R_b^w \omega_{ie}^b \quad (3.14)$$

where ω_{ie} is the angular velocity of earth rotation, A is the wander azimuth and ϕ is the latitude. The azimuth can be computed by

$$A = \tan^{-1} \left(\frac{\omega_{ie n}^w}{\omega_{ie e}^w} \right) \quad (3.15)$$

Roll and pitch are computed from the velocity output of the mechanization as (Lapucha, 1990)

$$\phi = \sin^{-1} \left(\frac{v^n}{\gamma \Delta t} \right) \quad (3.16)$$

$$\theta = \sin^{-1}\left(\frac{v^e}{\gamma\Delta t}\right) \quad (3.17)$$

where ϕ and θ are roll and pitch, respectively. v^n and v^e are the north and east velocities and γ is normal gravity. The accuracy of coarse alignment is usually at the level of 1 degree. The time needed for the coarse alignment largely depends on the time needed for the azimuth alignment, since the azimuth is sensed from the earth rotation which is of small magnitude.

3.4.2 Fine Alignment

Since the accuracy of the alignment largely determines the accuracy of subsequent results, the refinement of the initial attitude is very important. Fine alignment is generally done by a Kalman filter which models the misalignment error together with position error, velocity error, gyro drift and accelerometer bias. It is also assumed that the aircraft is stationary during the fine alignment process. The output velocities from the filter are used as measurements to update the filter. This process usually takes about 10 minutes since the azimuth direction usually takes a longer time to reach the required accuracy. For details of fine alignment see Wong (1985) and Liu (1992), for example.

For an INS installed on a small aircraft, it is necessary to average a few seconds of velocity estimated from the filter in order to average out the small movements of the aircraft due to wind or people's movement in the aircraft. This averaged

velocity is then used as update measurements in the filter. For details of such an algorithm see Wong (1985).

3.4.3 In-Flight Alignment

INS alignment can also be performed on a moving platform in real-time. GPS can provide real-time position and velocity information which can be used in-flight to align the INS. INS position and velocity errors can be estimated almost immediately from the comparison of position and velocity between the two systems. The speed and accuracy of attitude error estimation are determined partly by how long it takes the misalignment to propagate into position and velocity and partly by how easily the misalignment error can be separated from the sensor error such as gyro drift. When an INS experiences acceleration, the in-flight alignment will be much faster than during straight and level flight. For details see Tafel et al. (1983).

In this investigation, GPS double difference carrier phase measurements are used to continually update the INS in post-mission which is similar to in-flight alignment. The accuracy of the attitude error estimation will be refined during the flight especially when the aircraft experiences acceleration. However, in-flight alignment is not analyzed in this thesis.

CHAPTER 4

METHODOLOGY

This chapter reviews the Kalman filter algorithm. Modeling of the INS error states will be introduced as well as modeling of the error of the barometric height. The GPS/INS integration strategy, a cycle slip detection scheme under GPS-only system and GPS/INS integration system are discussed. An outline of the GPS/INS integration software developed for this thesis will also be given.

4.1 Kalman Filter Algorithm

The Kalman filter algorithm is well suited for this study since it can easily accommodate different sources of data. It is well documented in the literature, e.g. Gelb (1972) and Minkler et al. (1993). Kalman filtering consists of two processes, one is prediction and the other is updating. The first step is to predict one step in time according to the dynamic model. The updating process is to correct the predicted value with actual measurements according to their statistical weights.

The state model can be expressed as a first-order differential equation

$$\dot{x} = Fx + w \quad (4.1)$$

where x is the state vector of unknown parameters

F is the dynamics matrix

and w is the system noise.

If there is no system noise, the first-order homogeneous differential equation can be solved as

$$x_{k+1} = \Phi_{k+1,k} x_k \quad (4.2)$$

where $\Phi_{k+1,k}$ is the transition matrix between epoch k and epoch $k+1$. It can be computed as

$$\Phi = e^{F\Delta t} \quad (4.3)$$

If it is assumed that $\Delta t \rightarrow 0$, a simple form of Φ can be computed by only considering the first-order term when expanding the exponential function into a Taylor series, i.e.

$$\Phi \approx I + F \Delta t \quad (4.4)$$

The prediction equations can be written as

$$x_{k+1}(-) = \Phi_{k+1,k} x_k(+) \quad (4.5)$$

$$P_{k+1}(-) = \Phi_{k+1,k} P_k(+) \Phi_{k+1,k}^T + Q_k \quad (4.6)$$

where (-) represents the predicted value, (+) represents the updated value. P is the covariance matrix of the state vector and Q_k is the system noise which can be computed by the integral

$$Q_k = \int_k^{k+1} \Phi Q(\tau) \Phi^T d\tau \quad (4.7)$$

where $Q(\tau)$ is the system noise at time τ . If assuming $\Delta t \rightarrow 0$ and considering $\Phi \approx I + F\Delta t$, then Q_k can be simply expressed as (Schwarz et al., 1989)

$$Q_k \approx Q\Delta t \quad (4.8)$$

by ignoring the second order term of Δt . Q in the above equation is the spectral density matrix used in the filter. The elements of the spectral density matrix are selected to represent the inadequacy of the Kalman state vector to correctly model system dynamics.

The measurements can be modeled as

$$z = Hx + v \quad (4.9)$$

where z is the measurement vector, H is the design matrix and v is the measurement noise. The estimated state vector and its covariance from the update is

$$\hat{x}_{k+1}(+) = \hat{x}_{k+1}(-) + K \{ z_k - H \hat{x}_{k+1}(-) \} \quad (4.10)$$

$$P_k(+) = \{ I - K H \} P_k(-) \quad (4.11)$$

$$K = P_k(-) H^T \{ H P_k(-) H^T + R \}^{-1} \quad (4.12)$$

where \hat{x} is the estimated value, K is the Kalman filter gain and R is the covariance of the measurement noise.

4.2 INS Error Modeling

Since an INS will drift over time, modeling of the system errors is extremely important. There are many error sources from an INS; some can be estimated, others cannot. In this thesis, 15 error states are used, namely three position error states, three velocity error states, three misalignment states, three gyro drifts and three accelerometer biases (Wong, 1988, Lapucha, 1990, Cannon, 1991, Martell, 1991). They are expressed as a state vector

$$x = \{ \varepsilon_n, \varepsilon_e, \varepsilon_h, \delta\phi, \delta\lambda, \delta h, \delta v_n, \delta v_e, \delta v_h, d_n, d_e, d_h, b_n, b_e, b_h \}^T \quad (4.13)$$

where

$\varepsilon_n, \varepsilon_e, \varepsilon_h$ are the three misalignments in north, east and vertical directions, respectively (rad)

$\delta\phi, \delta\lambda, \delta h$ are the three position errors components in latitude, longitude and height respectively (m)

$\delta v_n, \delta v_e, \delta v_h$ are the three velocity error components in north, east and upward directions respectively ($m s^{-1}$)

d_n, d_e, d_h are the three gyro drift components ($rad h^{-1}$)

and b_n, b_e, b_h are the three accelerometer biases ($m s^{-2}$)

The gyro drifts and accelerometer biases are modeled as first-order Gauss-Markov processes. The error equation of an INS can be expressed in the local-level frame as (Wong, 1988)

$$\dot{\boldsymbol{\varepsilon}}^n = -\boldsymbol{\Omega}_{in}^n \boldsymbol{\varepsilon}^n - \delta\boldsymbol{\omega}_{in}^n + \mathbf{R}_b^n \mathbf{d} \quad (4.14)$$

$$\delta\dot{\mathbf{r}}^n = \mathbf{D}^{-1}\delta\mathbf{v}^n + \mathbf{D}^{-1}\mathbf{D}_r\delta\mathbf{r}^n \quad (4.15)$$

$$\delta\dot{\mathbf{v}}^n = -\mathbf{F}^n\boldsymbol{\varepsilon}^n - (2\boldsymbol{\Omega}_{ie}^n + \boldsymbol{\Omega}_{en}^n)\delta\mathbf{v}^n + \mathbf{v}^n(2\delta\boldsymbol{\omega}_{ie}^n + \delta\boldsymbol{\omega}_{en}^n) + \delta\boldsymbol{\gamma}^n + \mathbf{R}_b^n \mathbf{b} \quad (4.16)$$

$$\dot{\mathbf{d}} = -\alpha\mathbf{d} + \mathbf{w}_d \quad (4.17)$$

$$\dot{\mathbf{b}} = -\beta\mathbf{b} + \mathbf{w}_b \quad (4.18)$$

where

$$\mathbf{D}_r = \begin{pmatrix} 0 & 0 & -\dot{\phi}/(M+h) \\ \dot{\lambda}\tan\phi & 0 & -\dot{\lambda}/(N+h) \\ 0 & 0 & 0 \end{pmatrix} \quad (4.19)$$

The angular velocity errors $\delta\boldsymbol{\omega}_{ie}^n$, $\delta\boldsymbol{\omega}_{en}^n$, $\delta\boldsymbol{\omega}_{in}^n$ and normal gravity computation error $\delta\boldsymbol{\gamma}^n$ are functions of position and velocity errors. After expanding all errors in component form, the dynamics matrix of the model can be derived. See Wong (1988) for derivation details. The dynamics matrix is shown below

0	$-\omega \sin \phi$	$-\dot{\phi}$	$\omega \sin \phi$	0	0	0	$-\cos \phi$	0	R21	R22	R23	0	0	0
$\omega \sin \phi$	0	$-\omega \cos \phi$	0	0	0	1	0	0	R11	R12	R13	0	0	0
$\dot{\phi}$	$\omega \cos \phi$	0	$-\omega \cos \phi$	0	0	0	$-\sin \phi$	0	R31	R32	R33	0	0	0
0	0	0	0	0	0	1	0	0	0	0	0	0	0	0
0	0	0	0	0	0	0	1	0	0	0	0	0	0	0
0	0	0	0	0	0	0	0	1	0	0	0	0	0	0
0	$-\frac{f^u}{M}$	$\frac{f^e}{M}$	0	0	0	0	$\omega \sin \phi$	$-\frac{\dot{\phi}}{M}$	0	0	0	$\frac{R21}{M}$	$\frac{R22}{M}$	$\frac{R23}{M}$
$\frac{f^u}{R_E}$	0	$\frac{f^n}{M}$	0	0	0	$2\omega \tan \phi$	0	$-\frac{2\omega}{N}$	0	0	0	$\frac{R11}{R_E}$	$\frac{R12}{R_E}$	$\frac{R13}{R_E}$
$-f^e$	f^n	0	0	0	c	$2M\dot{\phi}$	$2R_E\omega \cos \phi$	0	0	0	0	R31	R32	R33
0	0	0	0	0	0	0	0	0	$-\alpha$	0	0	0	0	0
0	0	0	0	0	0	0	0	0	0	$-\alpha$	0	0	0	0
0	0	0	0	0	0	0	0	0	0	0	$-\alpha$	0	0	0
0	0	0	0	0	0	0	0	0	0	0	0	$-\beta$	0	0
0	0	0	0	0	0	0	0	0	0	0	0	0	$-\beta$	0

(4.20)

where

R_E is the earth radius (m)

M, N are the meridian and prime vertical radii of curvature, respectively (m)

ω is the angular velocity of earth rotation (rad s^{-1})

$c = \frac{2\gamma}{R_E}$ γ is the normal gravity (m s^{-2})

R_{ij} is the i -th row and j -th column of rotation matrix R_n^b

f^n, f^e, f^u are the specific force in north, east and vertical directions, respectively (m s^{-2})

and α, β are the correlation lengths of the gyro drifts and accelerometer biases (s).

The state transition matrix can be computed from the above dynamics matrix according to Equation (4.4) and can be used with the initial conditions of the state vector. The INS cannot maintain high accuracy trajectory, however when GPS carrier phase measurements are available as update measurements, the state vector can be precisely estimated using the Kalman update equations.

4.3 Vertical Channel Aiding

As previously discussed, an independent height source is needed to stabilize the vertical channel in real-time operation. A barometer is one choice which is inexpensive and convenient to use. However the accuracy of the barometric height is affected by many factors such as the aircraft dynamics and temperature changes, so careful modeling is very important.

The error equation associated with the vertical channel can be derived from the vertical mechanization. If the difference between the true height and barometric height is evaluated, it is found that the differences between these two heights are correlated to the height itself. Therefore a scale factor is added as an error state and is modeled as a first-order Gauss-Markov process. The error equation of the vertical channel is given below

$$\delta \dot{h} = \delta v^u - K_1 (\delta h - \mu H) \quad (4.21)$$

$$\delta \dot{v}^u = \delta a^u + \delta a_b + K_2 (\delta h - \mu H) \quad (4.22)$$

$$\delta \dot{a}_b = K_3 (\delta h - \mu H) \quad (4.23)$$

$$\dot{\mu} = -\frac{1}{\tau} \mu + w \quad (4.24)$$

where

δh	is the height error (m)
δv^u	is the vertical velocity error (m)
δa^u	is the vertical acceleration error (m s ⁻²)
δa_b	is the barometric acceleration error (m s ⁻²)
μ	is the barometric height scale factor error
H	is the aircraft height above ground, equals approximately to present height minus the initial height (m)
τ	is the correlation length of the scale factor (m)

and K_1, K_2, K_3 are three gains.

The barometric acceleration error δa_b and the barometric height scale error μ are introduced to the Kalman filter as additional error states together with the basic 15 error states to bring the total number of states to 17.

4.4 GPS/INS Integration

From the previous discussion, it is known that INS alone cannot achieve highly accurate position, velocity and attitude information while GPS alone cannot provide high accuracy attitude. Therefore the integration of GPS and INS is necessary. There are two ways of integration, namely the centralized filter which integrates GPS carrier phase measurements with INS gyro and accelerometer output (Cannon, 1991) and the decentralized filter which integrates INS output and GPS output from their separate filters to a master filter (Wei et al., 1990). In

this study, a centralized filter was chosen since it gives a tighter integration of GPS and INS (Cannon, 1991).

In tests conducted for this thesis, the gyro and accelerometer raw output are not available. Updated position, velocity and attitude information cannot be fed back into the mechanization, thus a closed loop integration is not an option in this case. An open loop integration scheme (see Figure 4.1) was adopted instead (Upadhyay et al., 1982). However, there are two weaknesses in using an open loop scheme compared to a closed loop. Errors in the INS are too large for a linear assumption in the Kalman filter and the correct dynamics of the error states are difficult to model. Nevertheless, there is one advantage by using an open loop scheme, which is that the filter is more stable with respect to poor data in an individual system.

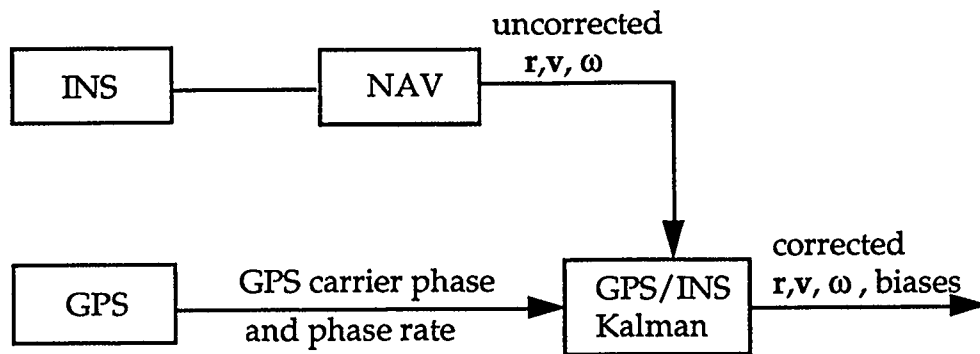


Figure 4.1

Concept of an Open-Loop GPS/INS Integration

The integration procedure is as follows (see Figure 4.2, Cannon, 1991; Sun et al., 1994): first, an INS prediction is performed at an interval given by the INS data until the INS time tag and GPS time tag match, then the GPS double difference carrier phase is computed. The double difference carrier phase is compared with

the predicted values based on the INS predicted position. If the difference is larger than a threshold, then a cycle slip has been detected and is subsequently corrected. After correcting the double difference carrier phase data, they are used to update the INS in a centralized Kalman filter. Position, velocity and attitude information output from the update are the final GPS/INS integration results. This process is repeated until the end of the GPS or INS data.

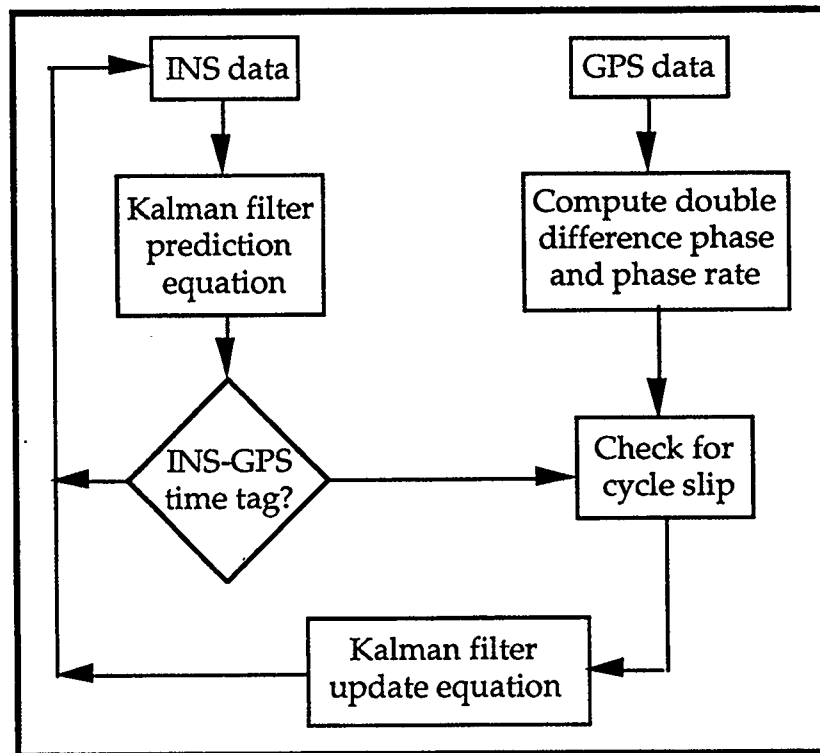


Figure 4.2
GPS/INS Integration Scheme

4.4.1 Cycle Slip Detection and Correction Algorithm

The occurrence of cycle slips is an important remaining problem in GPS carrier phase positioning. A cycle slip is a change of $\Delta \nabla N$ by an unknown integer number from one epoch to the next due to blockage of the signal path or signal noise (Lichtenegger et al., 1989). There are a number of ways to detect and correct cycle slips. Since an INS has a very good short-term stability, it can be used to detect GPS carrier phase cycle slips in a number of seconds depending on the performance of the INS, see for example Lapucha (1990), Loomis (1990), Cannon (1991) and Sun et al. (1994).

For the GPS only case, the detection of cycle slips can be done with the phase rate method which compares the measured carrier phase with the predicted carrier phase. The predicted carrier phase is computed by the phase rate from the equation (Cannon, 1987)

$$\Phi_{k+1} = \Phi_k + \frac{\dot{\Phi}_k + \dot{\Phi}_{k+1}}{2} \Delta t \quad (4.25)$$

where Φ is the carrier phase measurement (m), $\dot{\Phi}$ is the phase rate measurement (m s^{-1}) and Δt is the time interval between epoch k and $k+1$.

The accuracy of this method largely depends on the dynamics of the aircraft since it assumes that the velocity of the aircraft during Δt is constant which is not true in all cases, especially when the aircraft is taking off, landing or conducting special manoeuvres. Typically the accuracy of detectable cycle slips is about 10

cycles with this method under the normal aircraft dynamics and a 1 Hz data rate. Therefore an external source of information is needed to detect slips at the 1 cycle level.

The correction of cycle slips in the GPS-only case can be done using satellites in which cycle slips do not occur. However, at least four cycle slip free satellites are needed to keep a high accuracy trajectory of the aircraft. This correct trajectory can then be used to compute the double difference carrier phase which can then be compared with the measured one. The integer cycle portion of the difference can be considered as the number of cycles slipped.

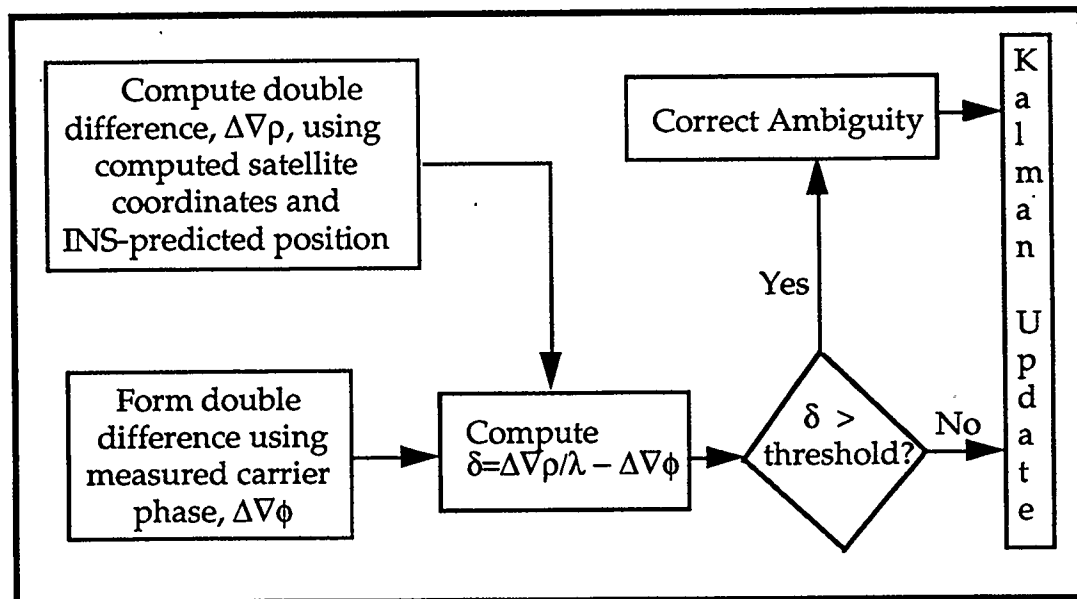


Figure 4.3
Cycle Slip Detection and Correction Scheme

One efficient way of detecting and correcting cycle slips when using GPS/INS is to use the INS to predict the position of the aircraft at the measurement epoch

based on the last epoch. A double difference carrier phase can then be computed from this predicted position (see Figure 4.3, Cannon, 1991). A difference can be formed by comparing the computed double difference with the measured one as shown in the following equation

$$\delta = \frac{\Delta\nabla\rho}{\lambda} - \Delta\nabla\phi \quad (4.26)$$

where

δ is the difference between the predicted double difference and the measured double difference in cycles

$\Delta\nabla\rho$ is the computed double difference in metres

$\Delta\nabla\phi$ is the measured double difference in cycles

and λ is the wavelength of the carrier phase.

A threshold has to be given to determine whether there is a cycle slip or not. This threshold should be smaller than 0.5 cycle in order to reliably detect small cycle slips. However, depending on the performance of the INS and the dynamics of the aircraft, this threshold may need to be loosened a little in order to avoid incorrect detection of cycle slips.

In this study, both cycle slip detection and correction schemes, namely GPS-only and GPS/INS integration approaches, are used to detect and correct cycle slips. The reason is that the prediction of the vertical channel in the INS used for this investigation is not good enough since the vertical channel is constrained to a barometric height or GPS single point positioning height. If only an INS is used to detect and correct the cycle slip, it is not always reliable since the height

prediction accuracy is not compatible with the accuracy of GPS double difference carrier phase measurements. However, if only GPS is used to detect the cycle slip, the carrier phase prediction using the phase rate may not be accurate enough since the dynamics of the aircraft could change quickly during the prediction interval. Therefore a combination of the two methods is used, i.e. when GPS has enough cycle slip free satellites available, GPS is used to correct the cycle slip and if GPS does not have at least four cycle slip free satellites, the INS is used to correct the cycle slip.

4.5 GPS/INS Integration Software

The GPS/INS integration software which implements the methods presented in the previous sections has been developed using C-language. This software is the FORTRAN version discussed in Cannon (1991) extended by the incorporation of vertical channel aiding. Figure 4.4 shows a brief flowchart of the software.

The first step in the software is to determine the GPS carrier phase integer ambiguities with static data, and also to perform the INS fine alignment with the zero velocity update (ZUPT) technique (Wong, 1985). After initialization, the INS begins to propagate to the next epoch and the GPS double difference carrier phase, satellite position, velocity are computed. This process continues until the time tags of the GPS and INS data match. The INS position, velocity and attitude are interpolated to this epoch, the error is propagated to this epoch using the Kalman prediction equation and then a GPS carrier phase update is then be performed. Before the update, cycle slip detection is performed using

both the GPS solution and the INS prediction. After correcting all cycle slips, the double differenced carrier phase data is used to update the INS using the Kalman update equations. This process continues until the end of either the GPS data or INS data.

This software can be run in a both forward and reverse-time processing manner. This capability gives flexibility to the software especially when the GPS data or INS data has a gap such that the first part of the data can be processed in a forward manner while the second part of the data can be processed in a reverse manner.

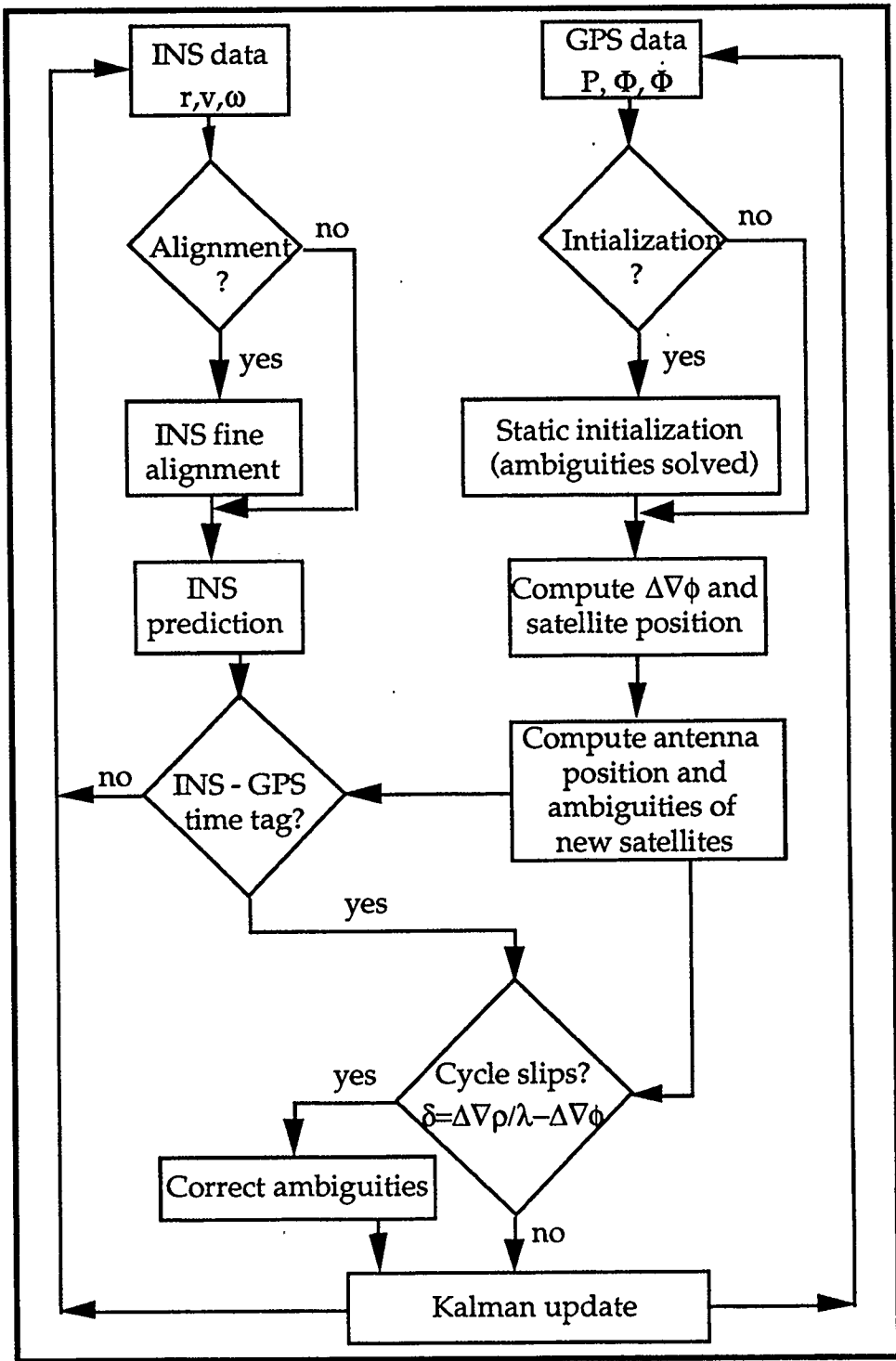


Figure 4.4
GPS/INS Integration Software Flowchart

CHAPTER 5

FLIGHT TESTING AND RESULTS

In this chapter, a series of flight tests will be used to verify the methodology discussed in Chapter 4. First the hardware that was used and the flight testbed are introduced. A flight test conducted over several days with multiple GPS antennas and an INS is outlined. A comparison of the attitude from the multi-antenna GPS system and the INS is summarized. Position, velocity and attitude results are given for two kinds of configurations, namely a strapdown configuration and a gimbal configuration. In order to relieve the GPS signal shading problem, the integration of the INS with multiple GPS antennas is analyzed.

5.1 Hardware Description

The testbed is a DCH-6 Twin Engine Otter Series 300 aircraft owned and operated by Sandia National Laboratories (SNL), Albuquerque, New Mexico (see Figure 5.1). It has a span of 19.81 metres, a length of 15.78 metres and a height of 5.67 metres.

There are several state-of-art navigation instruments onboard the Twin Otter, including a miniaturized Ring Laser Gyro Assembly (RLGA) Inertial Measurement Unit (IMU), NovAtel GPSCard™ 951R GPS receivers, Sandia Airborne Computer, SANDAC V, and real-time guidance and control facilities. An interferometric Synthetic Aperture Radar (IFSAR) is also installed in the aircraft (Fellerhoff et al., 1992).

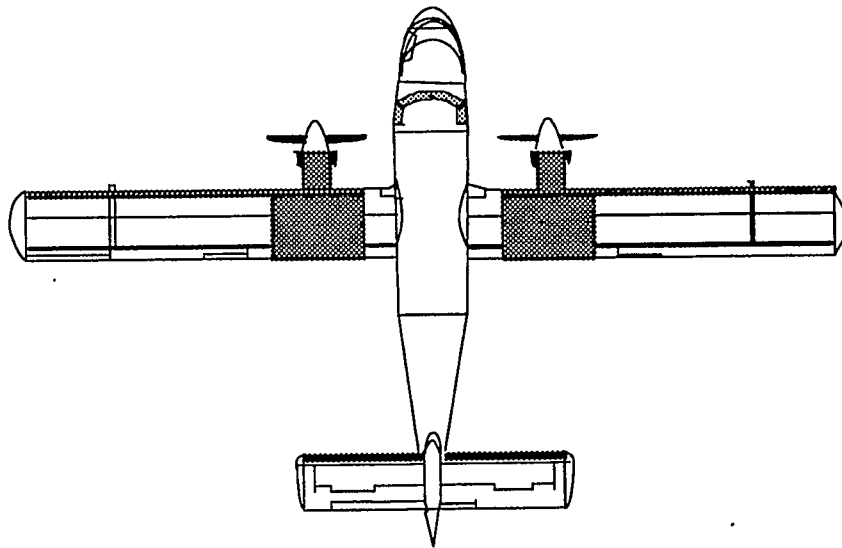


Figure 5.1
DCH-6 Twin Otter Series 300

The IMU is a cooperative product of SNL and the Space and Strategic Systems Group of Honeywell, Inc. It is attached to a 3-axis antenna pointing gimbal assembly near the synthetic aperture radar (SAR) antenna phase center. This installation isolates the IMU from the motion excited by the aircraft engine. The IMU is categorized in the 1 nm/hr class. It utilizes Honeywell GG-1320 gyros and Sundstrand QA-1200 accelerometers (Fellerhoff et al., 1992).

Each gimbal axis is driven by a DC torque motor and employs a synchro-resolver as a gimbal angle transducer. The filtered gyro data from the RLGA, supervisory command and gimbal angle measurements is input to the gimbal control calculations. The gimbal control outputs are updated at a 1024 Hz rate. The IMU navigation calculation is performed at 512 Hz which allows the higher frequency antenna motion to be measured. A real time point positioning GPS/INS filter operates at 64 Hz to estimate errors in position, velocity and attitude. The INS can also be configured as a pure strapdown system. This allows the system to be used for various applications (Fellerhoff et al., 1992).

The GPS receiver used in this investigation is the NovAtel GPSCard™ 951R model (Van Dierendonck et al., 1992). It is a C/A code, single frequency 10-channel GPS system which uses narrow-correlator spacing technology for improving code resolution and multipath reduction. The receiver can output raw pseudorange, carrier phase and phase rate which can be used for this application. The accuracy of the code is 10 centimetres (Lachapelle et al., 1993). The GPSCard™ can output raw data up to a 10 Hz rate. It can be inserted into a free ISA expansion slot of a desktop or laptop computer. Many tests and applications have demonstrated that metre-level accuracy can be achieved by using GPSCard™ pseudoranges (Lachapelle et al., 1994; Tiemeyer et al., 1994) while cm-level accuracies can be achieved using the GPSCard™ carrier phase measurements (Lachapelle et al., 1993).

Time tagging of INS is through a GPS PPS output from a TI-receiver in real-time operation. The accuracy is about 1-2 milliseconds.

5.2 Test Description

Many tests have been performed using the GPS/INS system, some in strapdown configuration and some in gimbal configuration. One multi-day test during February 1-4, 1994 is used to illustrate the algorithm in the strapdown configuration, and a one-day test on June 20, 1994 is used to illustrate the algorithm for the gimbal configuration. During the February test, four GPS receivers were installed on the aircraft in order to test the attitude determination capability of a non-dedicated multiple GPS receiver attitude system (Cannon et al., 1994). The attitude from this multiple GPS antenna system can be compared with the INS attitude which is of much higher accuracy. The layout of the antennas on the aircraft is shown in Figure 5.2.

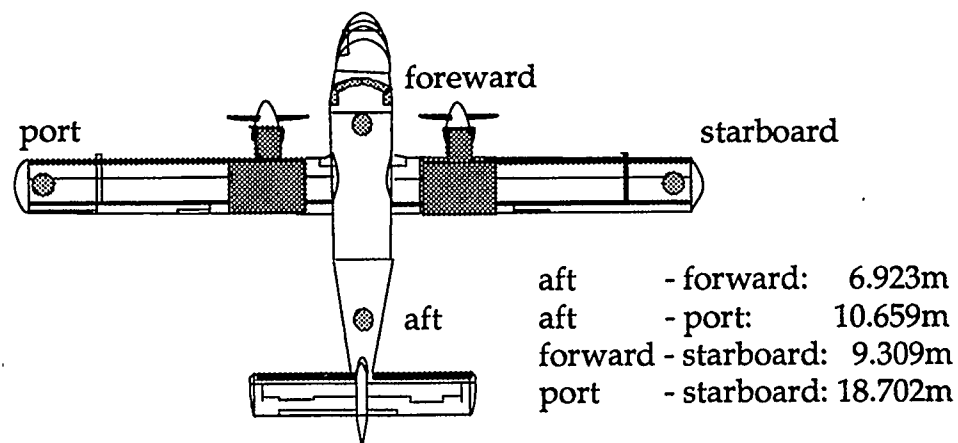


Figure 5.2

Layout of Aircraft GPS Antennas During the February Test

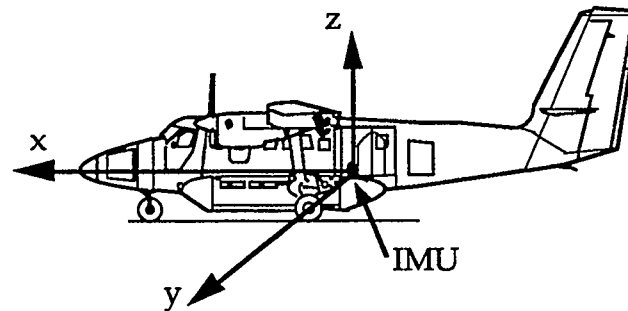


Figure 5.3
RLGA IMU Location

The RLGA IMU as well as the SANDAC are located on the floor of the aircraft just forward of the main cabin door, see Figure 5.3. Distances between the IMU and the antennas are listed in Table 5.1.

Table 5.1 Distances Between the Four GPS Antennas and the IMU During the February Test

Antenna	Distance (m)
forward	2.950
aft	4.524
port	9.750
starboard	9.406

One flight was conducted each day during the campaign. Each flight lasted from 1 to 2 hours. The INS data rate varied from 4 to 10.67 Hz while the GPS data rate ranged from 1 to 10 Hz over the different days. During the test period, there were 24 GPS satellites available. The number of satellites observed at the monitor

station on February 1 test is shown in Figure 5.4. Satellites observed during other test days were similar to Figure 5.4. The satellites observed at antennas on the aircraft varied from four to eight on February 1. Satellites observed at other days will be discussed in Sections 5.3 and 5.5. The height of the aircraft varied from 1600 to 5000 metres and the speed reached up to 100 m s^{-1} . One ground reference receiver was located about 50 metres from the aircraft during the static period. A GPSCard™ together with chokering was used at the ground receiver. The maximum separation between the monitor and aircraft was about 70 kilometres.

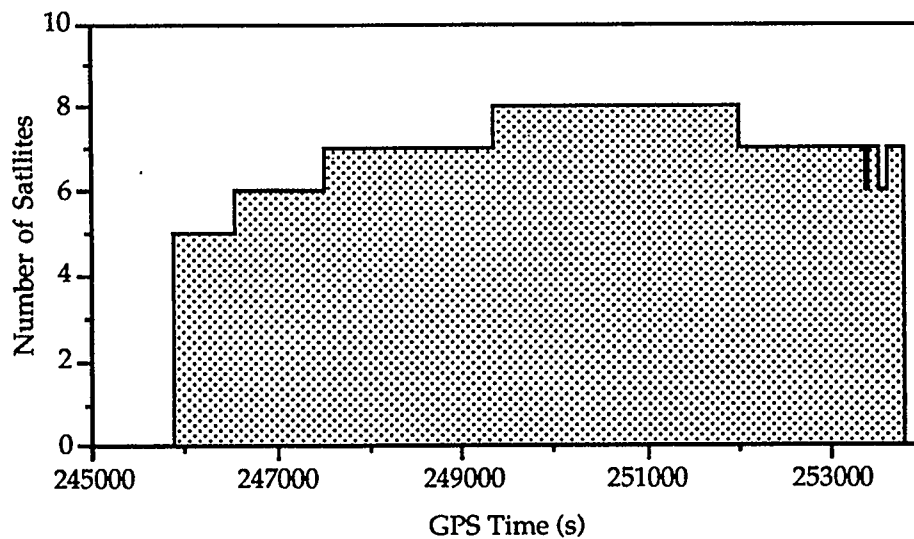


Figure 5.4
Satellites Observed at the Monitor Receiver During the February 1 Test

5.3 Comparison Between Attitudes from a GPS Multiple Antenna System and an INS

GPS multi-antenna attitude systems have been a research topic for the last few years. According to the installation of antennas, these systems typically can be classified as the plane constrained (Wilson et al., 1992), line constrained (Schwarz et al., 1992; Diefes et al., 1993) and the free-layout antenna system (Lu et al., 1993). All of these systems use baseline constraints from a pre-flight survey to search for the carrier phase ambiguities quickly. After the ambiguities are resolved, the relative antenna positions in the local-level frame are computed. Then attitude is computed based on these relative antenna positions. One difference between the various systems is the antenna configuration. The plane constrained system requires four antennas in the same geometric plane. This configuration introduces another constraint during the ambiguity search, i.e. the fourth antenna should be in the same plane defined by the first three antennas. The line constrained system has at least three collinear antennas in the pitch and roll directions. The first two antennas are very close to each other, e.g. 15 centimetres apart, so that the search for ambiguities can be done instantly. The determined attitude from this short baseline can be projected along the baseline to determine the approximate position of the other antenna which forms the longer baseline. The accuracy of the attitude determined from the short baseline limits the accuracy of the projection. Therefore the separation of the antennas should be chosen carefully. For the free-layout antenna system, the antennas can be installed in any convenient place on the aircraft which generally easily results in longer baselines than the other two systems.

The accuracy of all attitude systems is dominated by the antenna separation as well as multipath effects. From a theoretical point of view, assuming that the root mean square (RMS) of the baseline accuracy to be σ_b , the accuracy of the attitude can be expressed as

$$\sigma_{\text{attitude}} = \frac{\sigma_b}{S_b} \quad (5.1)$$

where S_b is the baseline length.

The definition of the antenna platform frame is as follows: first an antenna is defined as the master antenna which is used as the origin of the frame. Another antenna along the aircraft fuselage is defined as the pitch antenna which forms the y-axis of the coordinate frame. A third antenna positioned in the roll direction is defined as the roll antenna which defines the x-axis of the coordinate frame. The z-axis is perpendicular to the plane formed by the above three antennas and forms a right-handed coordinate frame. It is shown in Figure 5.5 for the current investigation. The coordinates of the four antennas in the antenna platform frame are listed in Table 5.2. They are obtained from a static GPS survey.

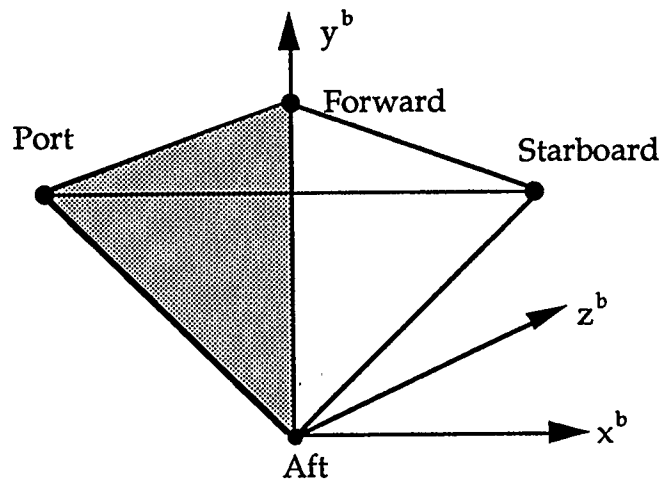


Figure 5.5
Antenna Platform Frame Definition

Table 5.2
Coordinates of the Four Antennas in the Antenna Platform Frame

Antenna	x-component (m)	y-component (m)	z-component (m)
1 (aft)	0.0	0.0	0.0
2 (forward)	0.0	6.9222	0.0
3 (port)	-9.5141	4.8085	0.0
4 (starboard)	9.1555	5.5115	0.9335

The free-layout antenna system is the most commonly used one since the installation of antennas is more flexible. This advantage is particularly important for airborne applications since the choice of antenna location on an aircraft is limited. In the methodology presented herein, it is assumed that the antennas are rigidly mounted on the aircraft. The antenna coordinates in the antenna platform

frame \mathbf{r}_b^i , defined by three antennas can be measured by a theodolite or by a GPS static initialization before a flight. The relative position of GPS antennas in the local-level frame \mathbf{r}_n^i can be measured by a GPS carrier phase solution with an accuracy of several millimetres. These two sets of coordinates should satisfy the following equation

$$\mathbf{r}_b^i = \mathbf{R}_n^b \mathbf{r}_n^i \quad (5.2)$$

where \mathbf{R}_n^b is the transformation matrix from the local-level frame to the antenna platform frame which can be expressed by the three attitude components roll, pitch and heading (φ, θ, ψ) as

$$\mathbf{R}_n^b = \begin{pmatrix} \cos\psi\cos\varphi - \sin\psi\sin\theta\sin\varphi & \sin\psi\cos\varphi + \cos\psi\sin\theta\sin\varphi & -\cos\theta\sin\varphi \\ -\sin\psi\cos\theta & \cos\psi\cos\theta & \sin\theta \\ \cos\psi\sin\varphi + \sin\psi\sin\theta\cos\varphi & \sin\psi\sin\varphi - \cos\psi\sin\theta\cos\varphi & \cos\theta\cos\varphi \end{pmatrix} \quad (5.3)$$

In Equation (5.2), the antenna platform frame coordinates and the local-level coordinates of the GPS antennas are known and the three attitude components are to be determined. This problem can be solved by minimizing the cost function

$$J(\varphi, \theta, \psi) = \|\mathbf{r}_b^i - \mathbf{R}(\varphi, \theta, \psi)\mathbf{r}_n^i\|^2 \quad (5.4)$$

by a least squares adjustment (Lu et al., 1993).

The February 4 test data was chosen for comparison between GPS and INS attitude results. The attitude of the aircraft during the mission is illustrated in Figure 5.6. Maximum roll and pitch were about 45 degrees and 12 degrees, respectively. The trajectory of the aircraft is shown in Figure 5.7. The PDOP and number of satellites observed for each antenna are given in Figures 5.8 and 5.9. During aircraft manoeuvres such as the 45 degree roll, the number of satellites observed at all four antennas are at least four although PDOP increases to 8. Therefore, attitude parameters were able to be obtained from the multi-antenna GPS attitude system during the entire flight. The test data was processed using the MULTINAV™ software package which estimates roll, pitch and heading using carrier phase measurements from three or more antennas (Lu et al., 1993). The INS attitude used as the reference is the attitude from the INS mechanization which has an accuracy of better than 1 arcmin for the roll and pitch components. The accuracy of heading is about 4-5 arcmins. However, the heading error is generally a bias which is removed during the comparison process.

In order to compare the GPS and INS attitude parameters, errors in the alignment of one system with respect to the other must be taken into account. The misalignment errors are inevitable due to the difficulties in mounting the systems in the aircraft. The rotation matrix that represents the mounting error is R_b^G which is the rotation required to transform the INS attitude parameters to the GPS antenna platform frame. It is computed as

$$R_b^G = R_b^n R_n^G \quad (5.5)$$

where R_b^n is the INS to local level transformation which can be formed using the INS output attitude parameters while R_n^G is the local level to GPS antenna platform frame transformation matrix which can be formed using attitude parameters computed from the GPS multi-antenna system. The matrix R_b^G is determined at each epoch of the flight data and then a mean transformation for the mission is determined.

Differences between the INS attitude and the multi-antenna attitude are shown in Figure 5.10. The RMS of differences in the pitch and heading directions are 7.3 and 3.9 arcmins which agree very well with previous results using a non-dedicated GPS attitude determination system, e.g. Lu et al. (1993). From Figure 5.10, it can be seen that differences in the aircraft roll increase by about 40 arcminutes when the aircraft takes off, and then maintains a consistent offset during the flight. It decreases again when landing. This large jump is due to the rigid body assumption for the antenna platform frame. In airborne applications, the wings flex during take-off, flight and landing. Therefore the defined antenna platform frame which includes the wing antennas will also change, so the attitude will also refer to a different reference frame. A similar comparison done in the marine environment (Lachapelle et al., 1994) in which structural flexing was not present, does not show these discontinuities.

In order to get a rigid body frame, wing flexure has to be removed before computing attitude so that the computed attitude refers to the same rigid body frame. It is assumed herein that both wings exercise the same amount of flexure, and that the wing flexure is in the vertical direction only, i.e. the z-component in

the antenna platform frame. Therefore Equation (5.2) is expanded to give (Cohen et al., 1993)

$$\begin{pmatrix} x^b \\ y^b \\ z^b \end{pmatrix} = \mathbf{R}_n^b \begin{pmatrix} x^n \\ y^n \\ z^n \end{pmatrix} + \begin{pmatrix} 0 \\ 0 \\ f \end{pmatrix} \quad (5.6)$$

where f is the wing flexure. For antennas mounted on the fuselage, f is equal to 0. Equation (5.6) can be solved using a least squares adjustment by minimizing the cost function

$$J(\varphi, \theta, \psi, f) = \left\| (\mathbf{r}^{b0} + \mathbf{B}_f f) - \mathbf{R}_n^b \mathbf{r}^n \right\|^2 \quad (5.7)$$

where \mathbf{B}_f is the flexure matrix defined as

$$\mathbf{B}_f = \begin{pmatrix} 0 & 0 & 0 \\ 0 & 0 & 0 \\ 1 & 0 & 1 \end{pmatrix}. \quad (5.8)$$

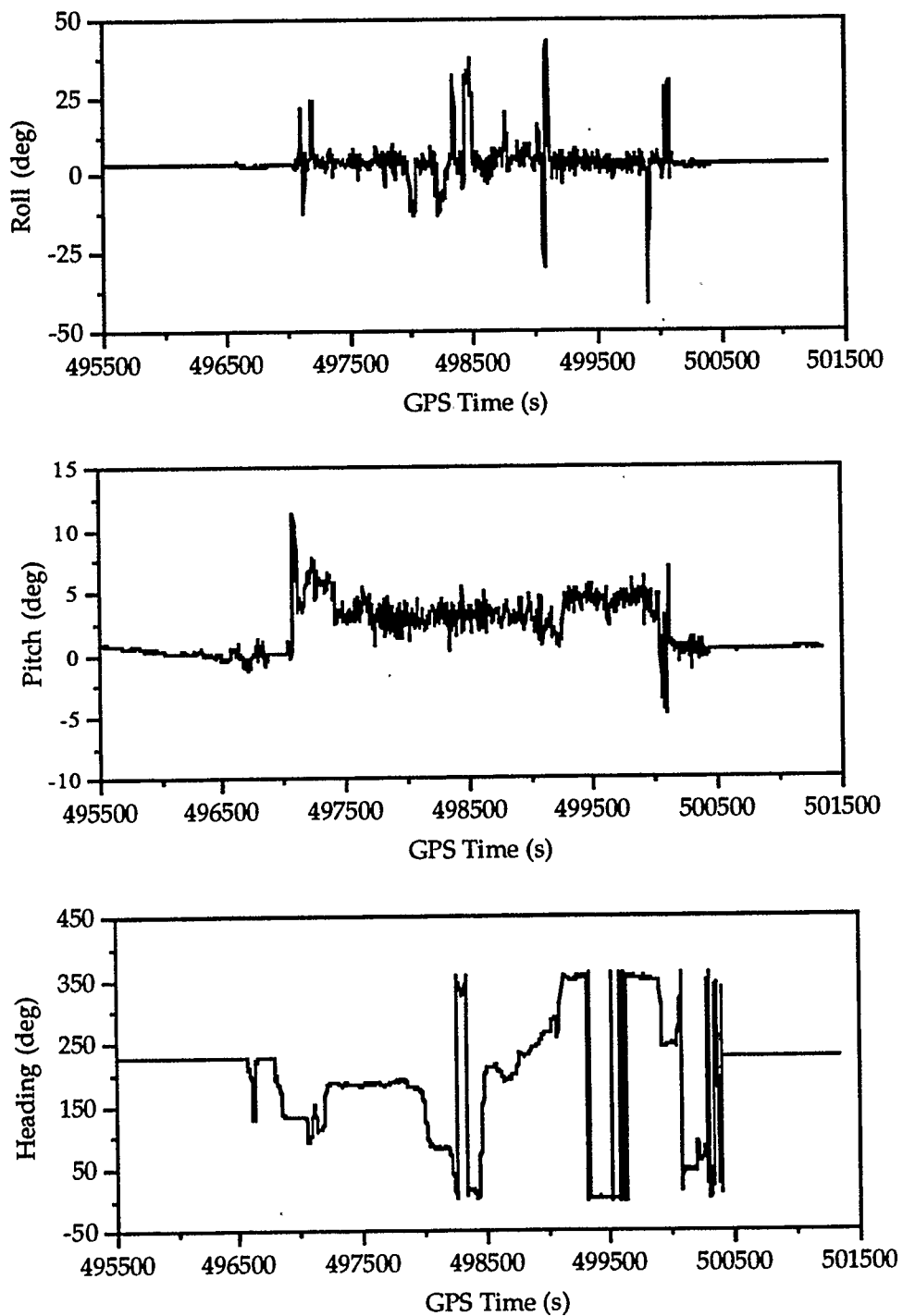


Figure 5.6
Aircraft Attitude From the GPS Multi-Antenna System
During the February 4 Test

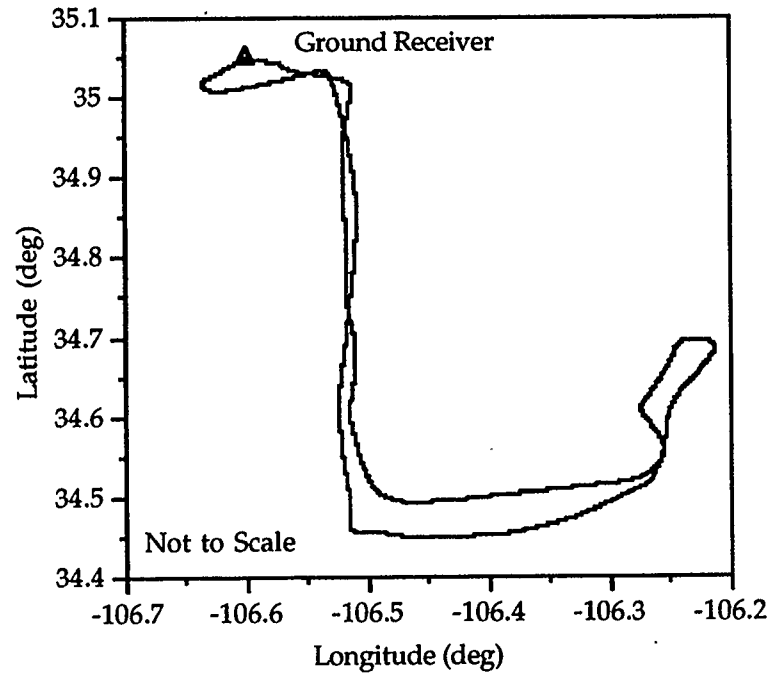
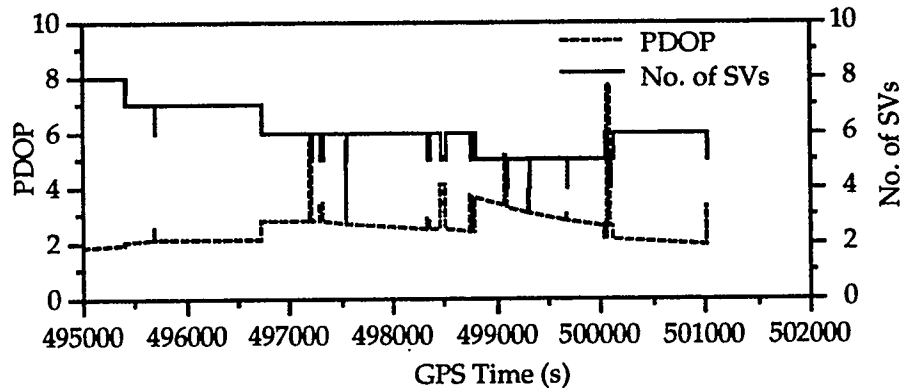
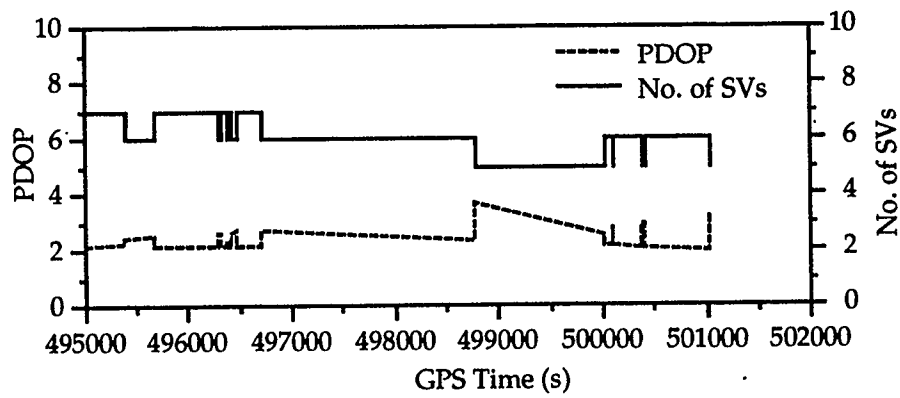


Figure 5.7
Aircraft Trajectory During the February 4 Test

In order to solve this equation without singularities, there must be at least one antenna on each wing to provide enough information to determine aircraft roll and wing flexure simultaneously. This means that there must be four antennas in total to determine roll, pitch, heading and wing flexure.

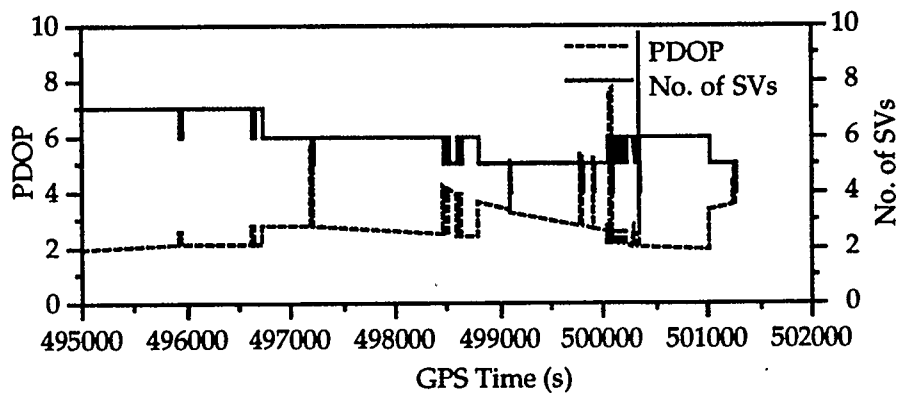


(a) Forward Antenna

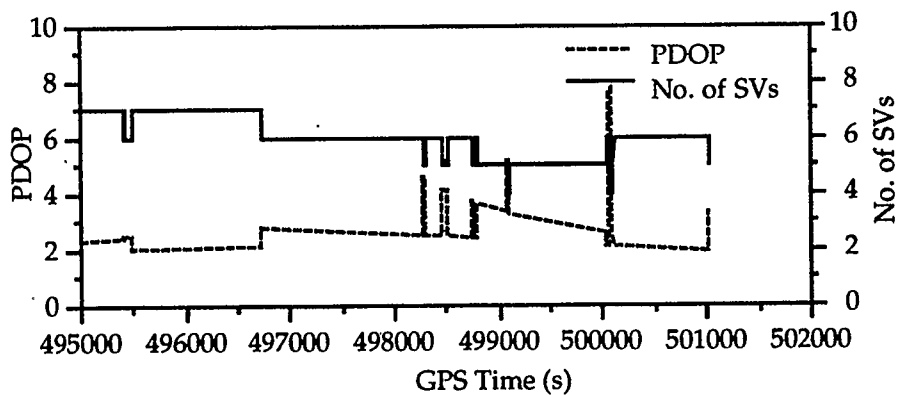


(b) Aft Antenna

Figure 5.8
PDOP and Number of Satellites Observed
at Forward and Aft Antennas During the February 4 Test



(c) Port Antenna



(d) Starboard Antenna

Figure 5.9
PDOP and Number of Satellites Observed
at Port and Starboard Antennas During the February 4 Test

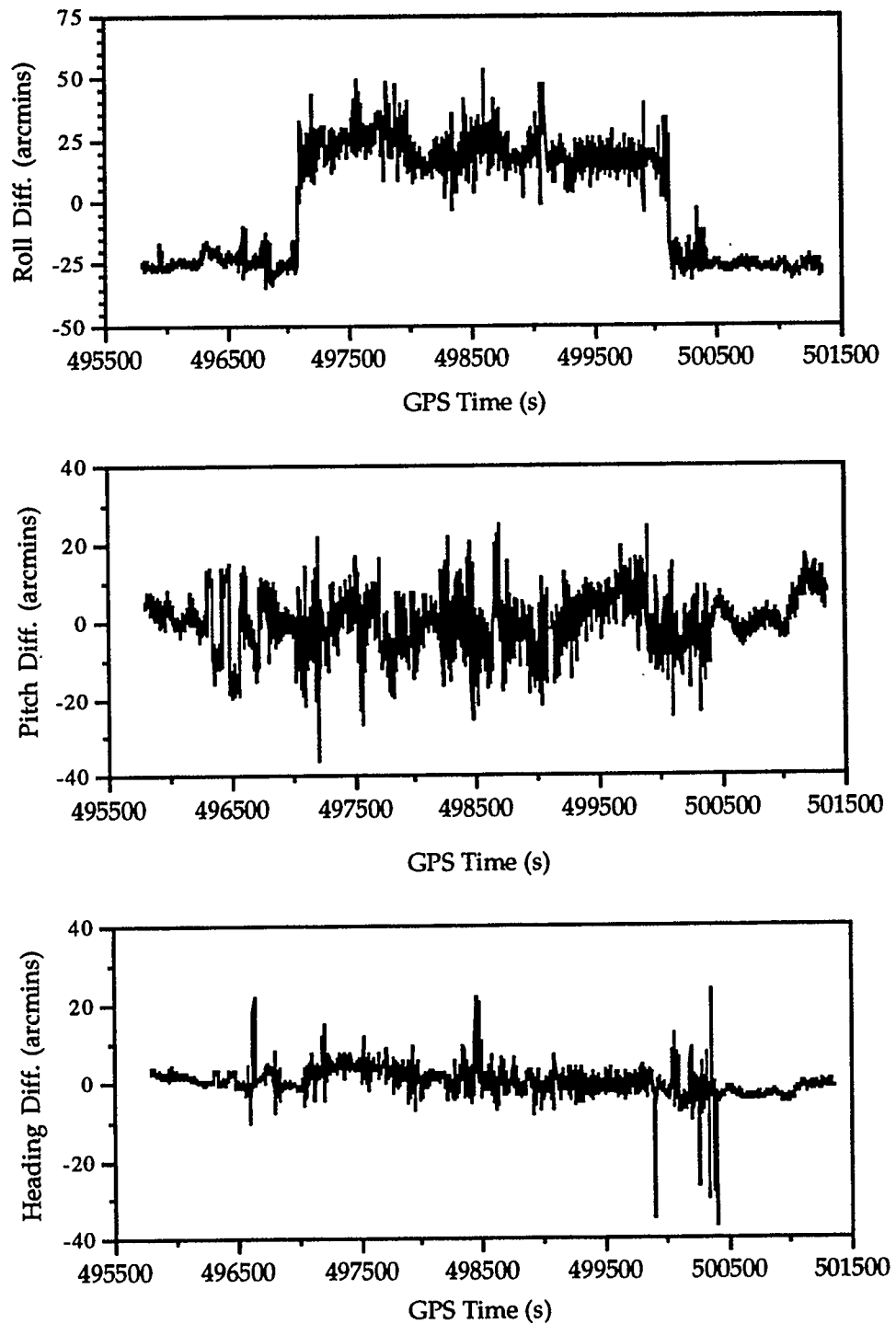


Figure 5.10
Roll, Pitch and Heading Differences Between Attitude from a GPS
Multiple Antenna System and an INS for the February 4 Test

The February 4 test data was reprocessed using the expanded model with wing flexure. Revised attitude differences between the GPS multi-antenna system and the INS are shown in Figure 5.11. The RMS of attitude differences before removing wing flexures are 23.3, 7.3 and 3.9 arcmins for roll, pitch and heading, respectively while the RMS of attitude differences after removing wing flexure are 5.0, 6.6 and 3.9 arcmins, respectively. Comparing the statistics before and after removing wing flexure, the roll differences are obviously smaller, but pitch is also improved to some extent. That is due to the coupling of the attitude components in the transformation matrix. Results from February 3 are similar, see Cannon et al. (1994).

Statistics of the attitude differences before and after wing flexure modeling are summarized in Table 5.3. From this table, it can be seen that the accuracy of the roll is improved significantly. After removing the wing flexure, the magnitude of the RMS varies from 3.9 to 6.6 arcmins. This accuracy is also comparable with results from other dedicated attitude system, see e.g. Schade et al. (1993).

Table 5.3
RMS of the Differences Between Attitude From
a Multi-Antenna GPS System and an INS

	RMS of Differences (arcmins)		
	Roll	Pitch	Heading
Without Wing Flexing Model	23.3	7.3	3.9
With Wing Flexing Model	5.0	6.6	3.9

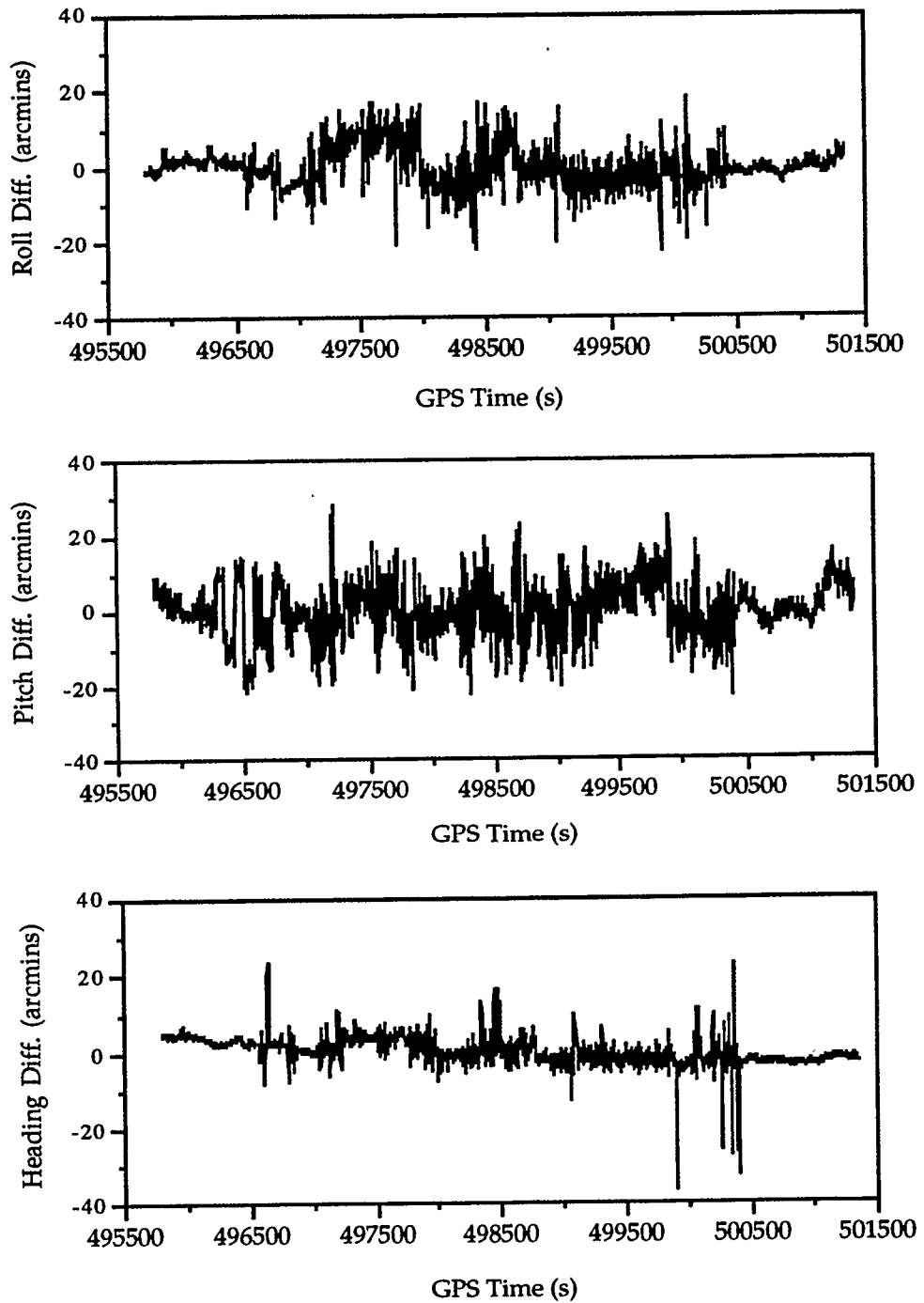


Figure 5.11

Roll, Pitch and Heading Differences Between Attitude from a GPS Multi-Antenna System and an INS for the February 4 Test When Using a Wing Flexure Model

The actual wing flexure determined from the least squares adjustment is shown in Figure 5.12. As can be seen the maximum magnitude reaches 0.14 metres. The baseline length in the roll direction is about 10 metres and the magnitude of the roll jump is about 40 arcminutes (see Figure 5.10) which results in an approximate magnitude of wing flexure of 0.12 metres. This value is compatible with the magnitude derived from the least squares adjustment.

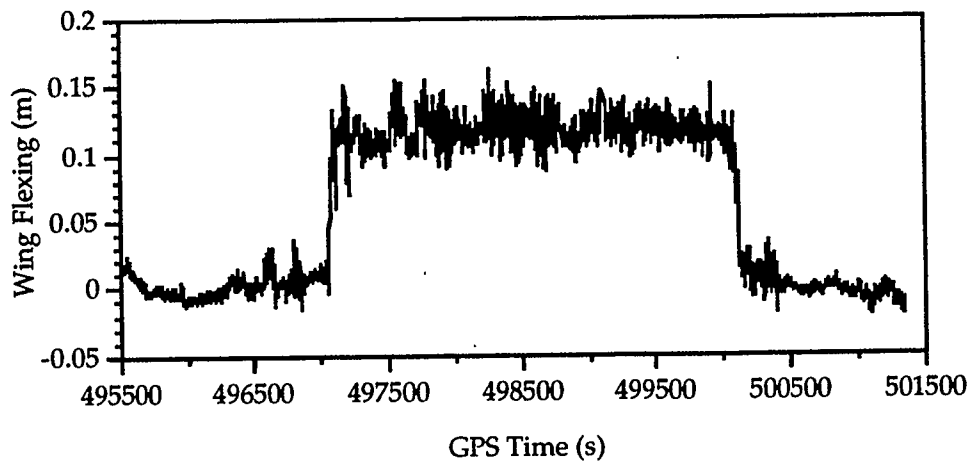


Figure 5.12
Wing Flexure of Aircraft During February 4

5.4 Positioning and Attitude Results from GPS/INS Integration

Many tests have been done using this set of hardware under these two types of configurations, namely strapdown and gimbal modes (Fellerhoff et al., 1992; Owen et al., 1992; Burgett, 1994; Cannon et al., 1994 and Sun et al., 1994). Results from these two modes are discussed in the following.

The spectral densities selected here are a representation of the inadequacy of the error states to correctly model aircraft dynamics. They are given in Table 5.4. These values are determined according to the performance of the gyro and the accelerometer.

Table 5.4
GPS/INS Kalman Filter Spectral Densities

Parameter	Spectral Density
Position	0
Velocity	$1.0 \cdot 10^{-6} \text{ m}^2 \text{ s}^{-3}$
Misalignments	$1.0 \text{ arcsec}^2 \text{ s}^{-1}$
Gyro Drifts	$1.4 \cdot 10^{-10} \text{ deg}^2 \text{ h}^{-3}$
Accel. Biases	$1.4 \cdot 10^{-10} \text{ m}^2 \text{ s}^{-5}$

5.4.1 Position and Attitude Results from the Strapdown Configuration

Data from the February 1 test is chosen for this investigation. Since the forward antenna is located closest to the IMU and is situated in the most stable location, it is used as the main antenna to verify the methodology. The aircraft trajectory during the mission is shown in Figure 5.13.

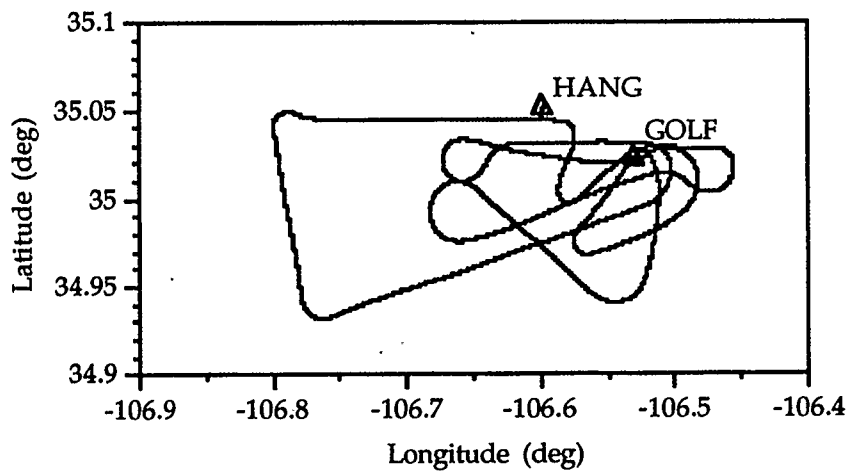


Figure 5.13
Aircraft Trajectory During the February 1 Test

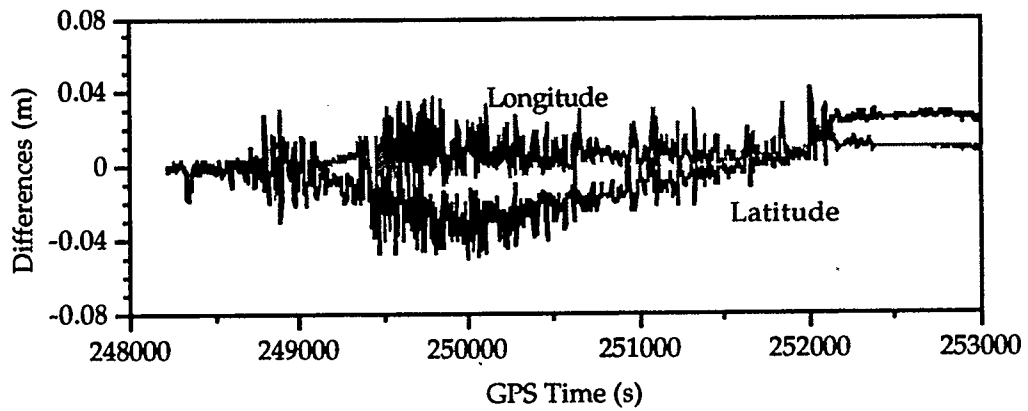
Before integration, GPS-only solutions are also computed using SEMIKIN™, a software package developed at The University of Calgary using double difference carrier phase to compute a kinematic trajectory of a vehicle (Cannon, 1990). Since there was data collection during the static periods before and after the flight, integer ambiguities of the double differenced carrier phase measurements could be solved using static data either before the flight or after the flight. A ground monitor receiver (HANG) was located about 150 metres from the aircraft during the static periods. Another ground receiver (GOLF) was located about 7 kilometres from the airport. In order to ensure the correctness of the GPS solution, different kinds of comparisons were performed (Sun et al., 1994). A comparison of the trajectories from forward and reverse time processing was done and the differences in all three components are less than 1 cm. A comparison of the static solution at the end of the flight from the forward run and the static solution using the static data at the end of the flight was also performed and the differences are below 1 cm in the three position components.

The residuals of the double difference carrier phase were also less than 3 cm. Aircraft trajectories computed from two ground reference stations, namely HANG and GOLF, were also compared. The statistics of the differences are listed in Table 5.5. After these procedures, the GPS solutions can be used for comparison with the GPS/INS integration results. The accuracy of the aircraft trajectory from GPS carrier phase solution is expected to be at the centimetre level given the above analysis.

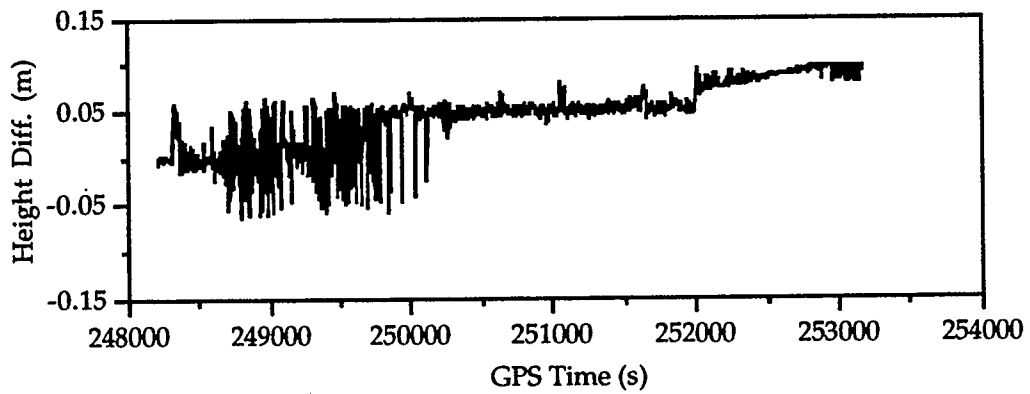
Table 5.5
RMS of the Differences Between Aircraft Trajectories
Computed from Two Ground Reference Stations

RMS (cm)		
Latitude	Longitude	Height
2.4	1.0	1.5

Position differences between the GPS-only solution and the GPS/INS integration solution are shown in Figure 5.14 when the barometric error model discussed in Section 4.3 is not used. After using the barometric error model, the revised position differences are shown in Figure 5.15.

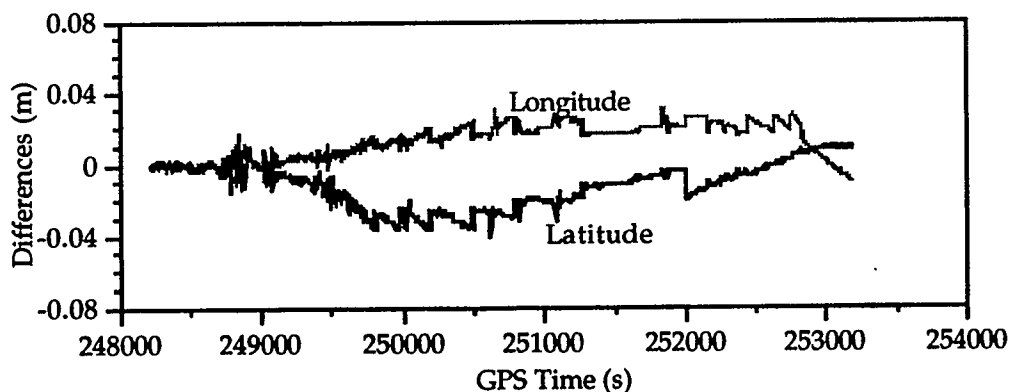


(a) Horizontal Components

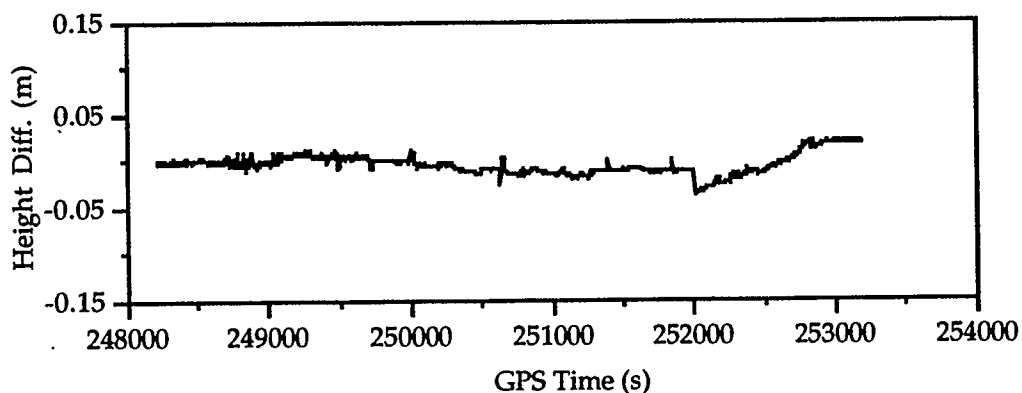


(b) Height

Figure 5.14
Position Differences Between the GPS-only Solution and
the GPS/INS Integration Solution During the February 1 Test
When No Barometric Model was used



(a) Horizontal Components



(b) Height

Figure 5.15
Position Differences Between the GPS-only Solution and
the GPS/INS Integration Solution During February 1 Test
When Using the Barometric Error Model

Statistics of the differences for latitude, longitude and height in the two cases are listed in Table 5.6. From the comparison, it can be seen that the accuracy of the horizontal components is not improved when adopting the barometric error model, however the height differences are reduced significantly. The reason is that the barometric height errors are largely correlated to the aircraft height as

can be seen from Figure 5.16. It shows the differences between the GPS height and the barometric height versus the differences between GPS height and the initial height of the aircraft.

Table 5.6
RMS of the Differences Between the GPS-only Positions and the GPS/INS Integration Positions for the February 1 Test

	RMS (metres)		
	Latitude	Longitude	Height
Without Baro Error Model	0.021	0.011	0.059
With Baro Error Model	0.017	0.016	0.013

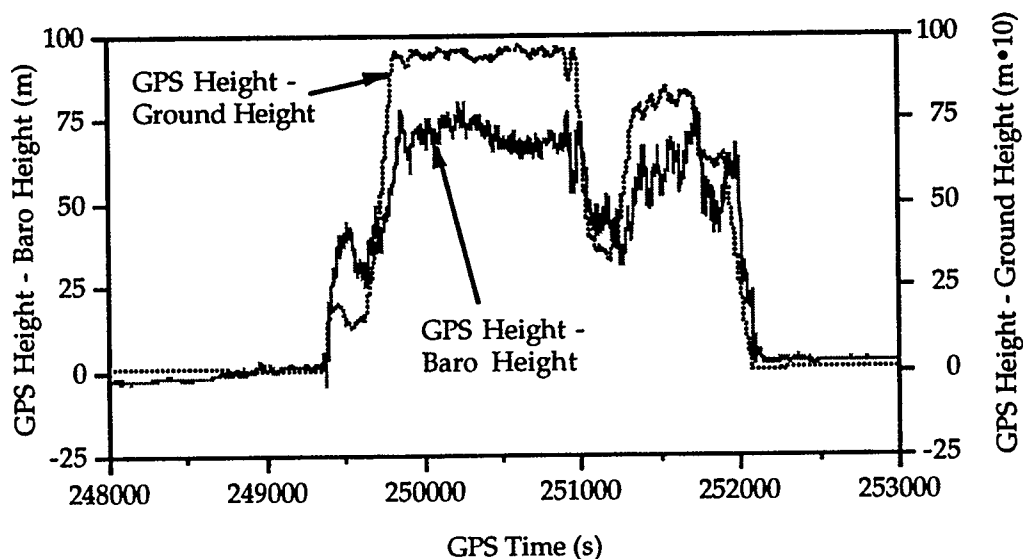


Figure 5.16
GPS Versus Barometric Height and GPS Versus Initial Aircraft Height During the February 1 Test

Velocity components are not compared in this study. The reason is that the velocity from the GPS/INS integration is the aircraft velocity at the IMU location. It is different from the velocity at the GPS antenna. This difference can reach the decimetre/second level. The angular velocity is needed to transform these two velocities. However, as mentioned before, raw angular velocity was not available during this investigation. The derived angular velocity from the attitude may introduce additional noise. Therefore the GPS-only velocity is not compared with results from the GPS/INS integration. Nevertheless, the velocity error states are estimated from the Kalman filter. They are plotted in Figures 5.17 and 5.18 for the horizontal and vertical components, respectively, for the February 1 test. From Figure 5.17, it can be seen that the horizontal velocity errors are very smooth as expected. The magnitude reaches 4 m s^{-1} . The discontinuities are generally correlated with aircraft turns. This may imply that there could be still time tagging error between the two systems. The vertical velocity error is very noisy due to the deployment of the barometric height as can be seen from Figure 5.18.

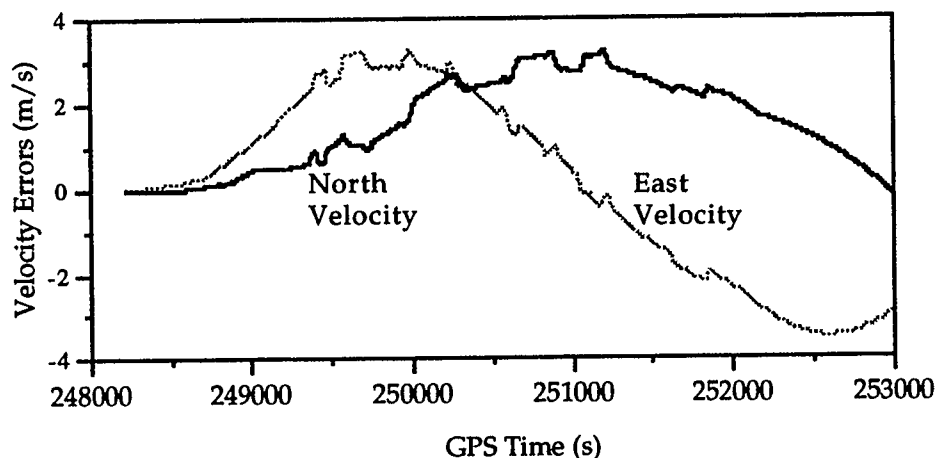


Figure 5.17
Horizontal Velocity Errors Estimated from
GPS/INS Integration for the February 1 Test

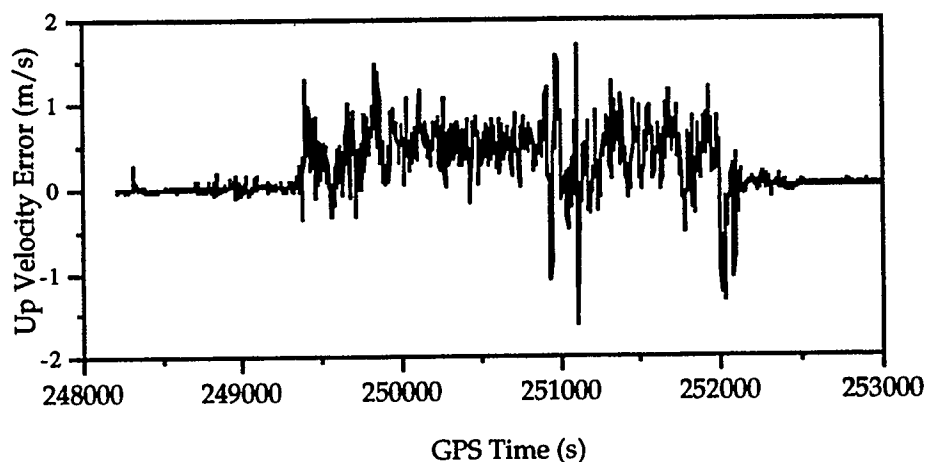


Figure 5.18
Vertical Velocity Error Estimated from
GPS/INS Integration for the February 1 Test

The estimation of the attitude error is also needed in this research. However, since no reference attitude is available for comparison, the accuracy of the attitude error estimated from GPS/INS cannot be evaluated. The horizontal attitude errors and the heading error for February 1 are given in Figures 5.19 and 5.20, respectively for February 1 test. The horizontal error states are very small as expected.

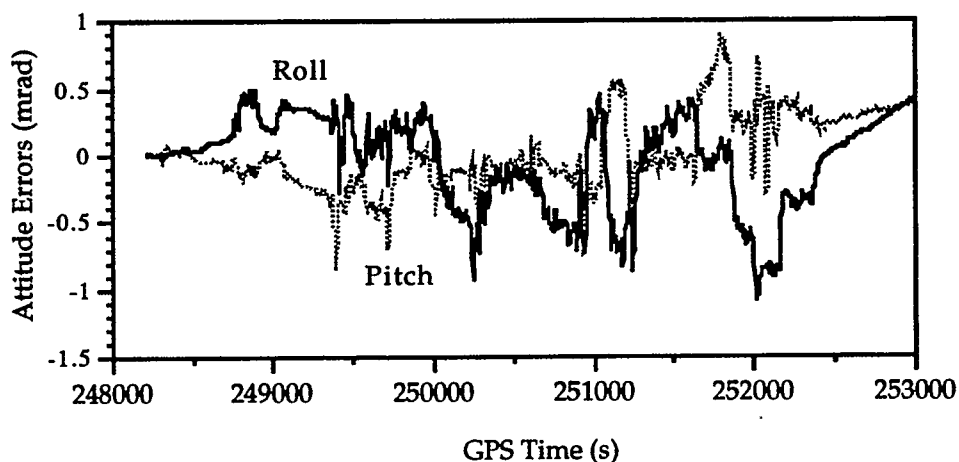


Figure 5.19
Horizontal Attitude Errors Estimated
from GPS/INS for the February 1 Test

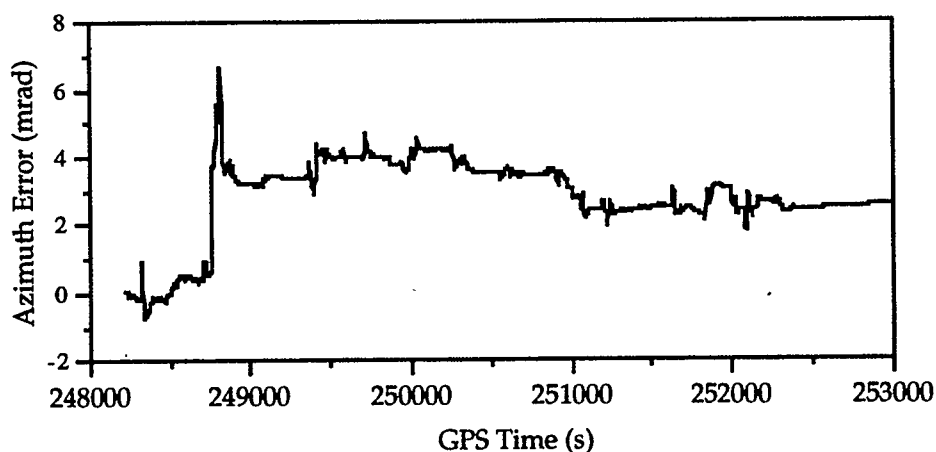


Figure 5.20
Heading Error Estimated from GPS/INS for the February 1 Test

After using the barometric error model, the horizontal and heading errors estimated from the GPS/INS integration are shown in Figures 5.21 and 5.22, respectively. Comparing these with Figures 5.19 and 5.20, it can be seen that attitude estimation is improved when the GPS/INS height agrees better with the GPS derived height. The magnitude of the estimated attitude error agrees better

with the performance of the INS when the barometric error model is applied. This phenomenon would not usually happen when position or velocity are used as the update measurements. One reason may be that carrier phase measurements, instead of positions, are used as the update measurements.

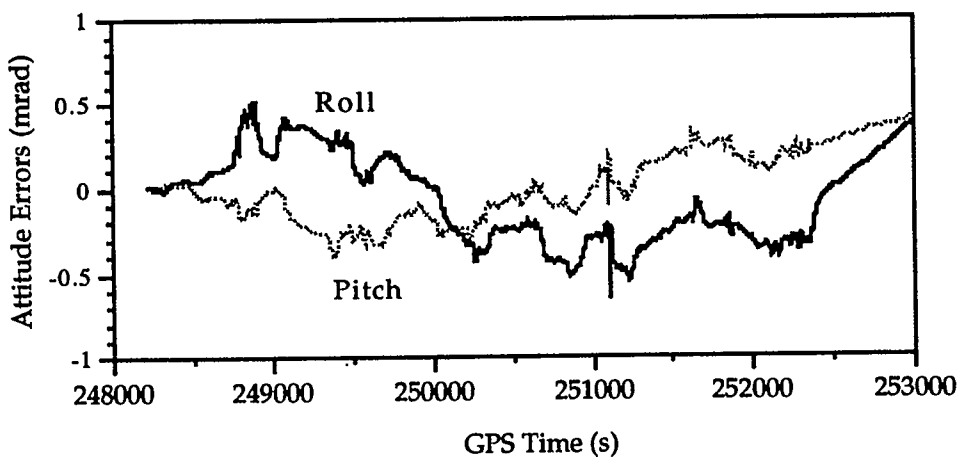


Figure 5.21

**Horizontal Attitude Errors Estimated from GPS/INS
for the February 1 Test when Using the Barometric Error Model**

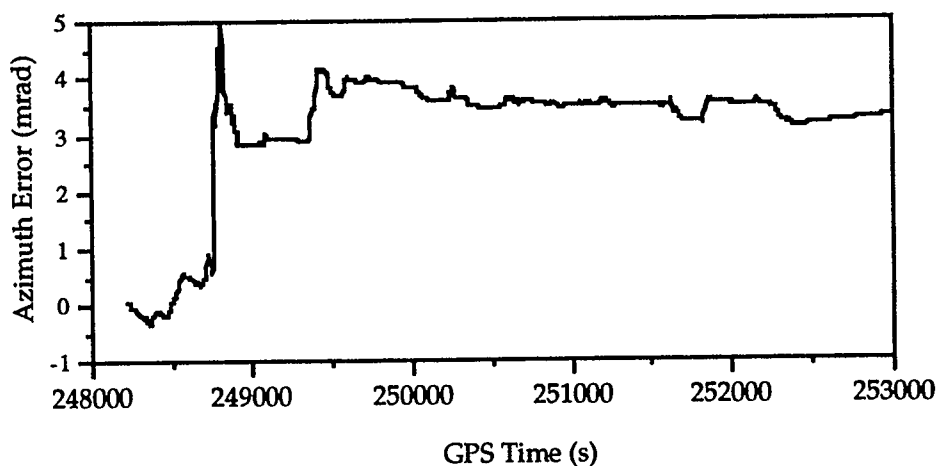


Figure 5.22

**Heading Error Estimated from GPS/INS
for the February 1 Test when Using the Barometric Error Model**

5.4.2 Position and Attitude Results from the Gimbal Configuration

In Sandia's SAR application, in order to isolate the high frequency vibration of the SAR antenna due to the noise from the aircraft engine, the IMU is installed directly on the SAR antenna (Fellerhoff et al., 1992). The IMU is situated on a three-axis gimbal in order to isolate the SAR antenna from aircraft movement.

The same 15 error states are used in the Kalman filter to estimate errors in INS position, velocity and attitude as in the strapdown case. However in this configuration, no baro-aiding data was recorded, therefore the barometric error model is not necessary in this case. Test data from one day, namely June 20, 1994, is used to show the GPS/INS integration results. The hardware used for this test was the same as that used in the February test except that only one GPS antenna was installed on the aircraft. The test was performed in the same area and the trajectory of the aircraft is shown in Figure 5.23. A ground reference station was set up at a distance about 7 km from the airport. During the test, GPS data was recorded at 1 Hz while INS position, velocity and attitude were recorded at 2 Hz. SAR data was also recorded during the test. There are some ground points whose coordinates are known. Another set of coordinates will be determined for these points from SAR data using position, velocity and attitude determined from GPS/INS integration (Burgett, 1994). By comparing the known coordinates and the SAR determined coordinates from GPS/INS position, velocity and attitude, the accuracy of the system can be determined. At present, as previously mentioned, a comparison can only be made between position results from GPS/INS and GPS-only results. Velocity and attitude errors are given also.

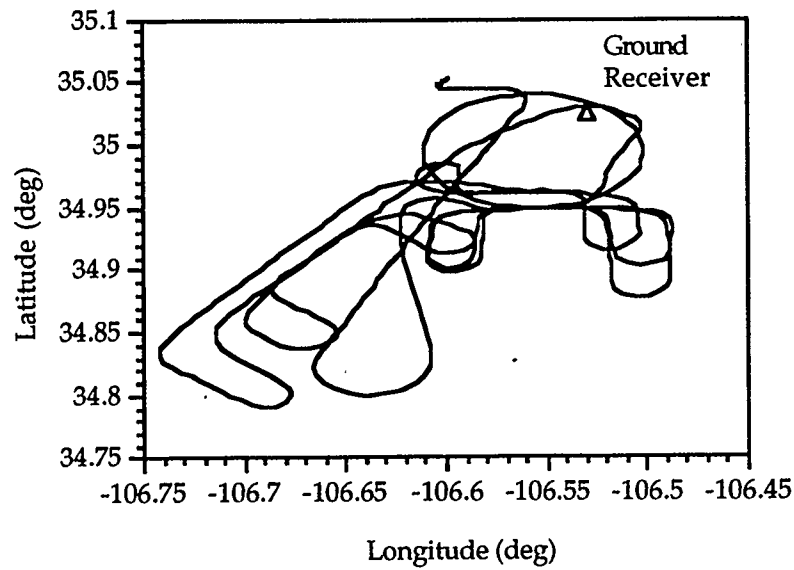


Figure 5.23
Aircraft Trajectory During the June 20 Test

Differences between the GPS-only and GPS/INS positions are shown in Figure 5.24 for the June 20 test data. From the figure, it can be seen that the magnitude of the differences is at the level of a few centimetres. The RMS of the differences are 1.7, 1.4 and 10.3 cm for latitude, longitude and height, respectively. This means that the position of the aircraft is mainly controlled by the GPS position since the update rate is at 1 Hz.

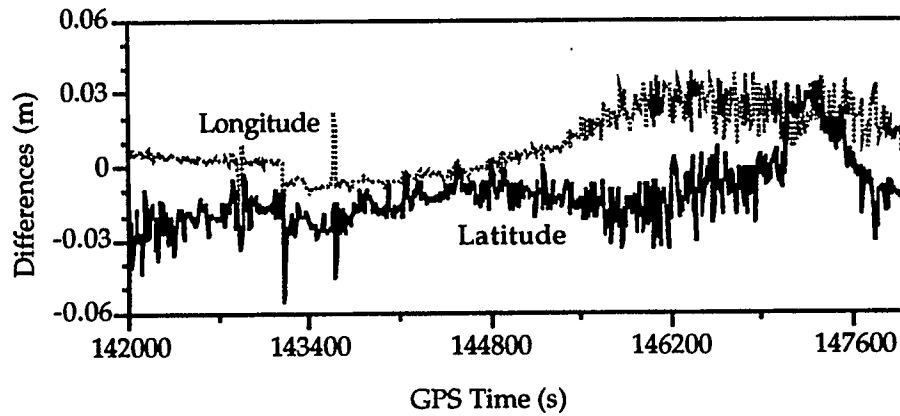


Figure 24
**Position Differences Between the GPS-only and
 the GPS/INS Positions for the June 20 Test**

Horizontal velocity errors estimated from the GPS/INS integration are given in Figure 5.25. The magnitude of the error is about 4 m/s and is very smooth. Horizontal attitude and heading errors estimated from the GPS/INS are illustrated in Figures 5.26, and 5.27 respectively. Again these errors are very smooth as expected.

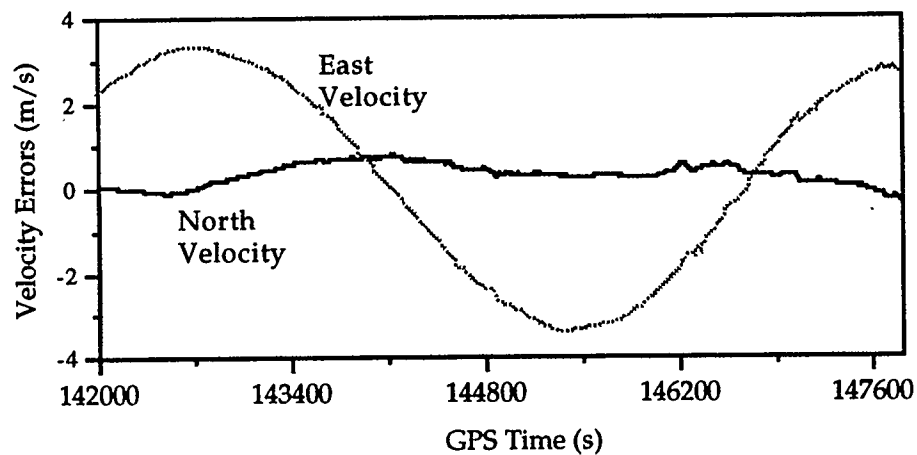


Figure 5.25
Horizontal Velocity Errors Estimated from GPS/INS for the June 20 Test

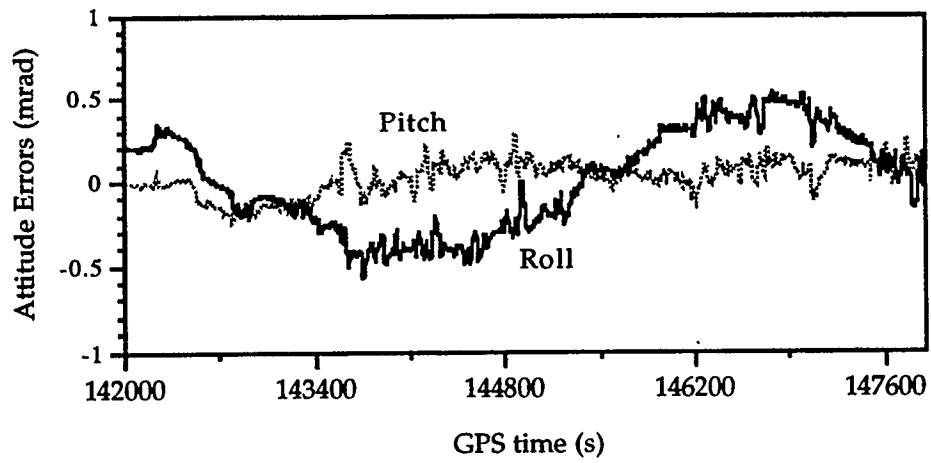


Figure 5.26
Horizontal Attitude Errors Estimated from
GPS/INS for the June 20 Test

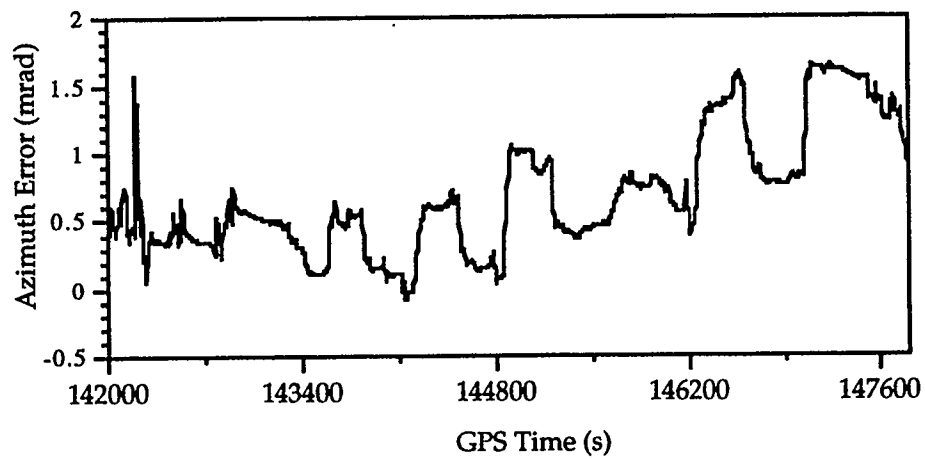


Figure 5.27
Heading Error Estimated from GPS/INS for the June 20 Test

5.5 Integration of INS with Multiple GPS Antennas

During some aircraft manoeuvres, such as sharp banked turns, some GPS signals may be shaded with respect to the antenna. If multiple antennas are installed on the aircraft, this shading may occur at one antenna, but may not occur at other antenna locations. Therefore, the utilization of multiple GPS antennas to integrate with an INS may alleviate the shading problem. This system can use positions from different antennas which were determined by differential carrier phase positioning with respect to a ground receiver separately, to keep the INS updated, maintain a high accuracy aircraft trajectory and attitude. With the reduction of receiver costs, as well as the increased demand for a high level of aircraft positioning accuracy, such a system may become operational in the future.

When integrating an INS with multiple GPS antennas, it is critical to accurately determine the lever arm correction of each antenna with respect to the INS. Otherwise, any error will distort the estimated INS attitude error. In the current multiple antenna system, the IMU body frame was not aligned with the aircraft platform frame, hence it is difficult to directly measure the precise lever arms. However, the positions of the four antennas in the local-level frame, \mathbf{r}_n^i can be computed from the GPS carrier phase solutions. As well, the attitude \mathbf{R}_n^b is known from the INS output. The distance between the IMU to each antenna can be measured accurately before the mission. Therefore the local-level position of the IMU, \mathbf{r}_n^b can first be computed using the distances to each antenna and their known local-level positions. From these local-level positions, the coordinate

differences between each antenna and the IMU, i.e. dN_n^i , dE_n^i , dH_n^i , can be computed in the local-level frame (in the north, east and vertical directions). These coordinate differences can now be transformed to the IMU body frame using the known attitude from INS, i.e.

$$\begin{pmatrix} dx_b^i \\ dy_b^i \\ dz_b^i \end{pmatrix} = \mathbf{R}_n^b \begin{pmatrix} dN_n^i \\ dE_n^i \\ dH_n^i \end{pmatrix} \quad (5.9)$$

Coordinates of the four antennas in the IMU body frame are listed in Table 5.7.

Table 5.7
GPS Antenna Coordinates in the IMU Body-Frame

Antenna	x (m)	y (m)	z (m)
forward	0.074	2.555	1.473
aft	-0.267	-4.354	1.200
port	-9.539	0.848	1.799
starboard	9.162	0.718	1.934

The February 2 test is selected for this investigation. The trajectory of the aircraft during the test is shown in Figure 5.28. The ground receiver is located about 50 metres from the aircraft during the initial static period. Since the environment for each antenna is different, the number of satellites observed at different antennas

varies. For this test, the number of satellites observed at the forward, aft and port antennas are given in Figure 5.29. From the figures it can be seen that the number of satellites observed varied from 2 to 8 for the forward antenna, always more than 4 for the aft antenna and from 3 to 8 for the port antenna. However, since the forward antenna is closest to the IMU and is in the most stable location, it is used as the master antenna to integrate with the INS. Therefore, in order to keep the INS accurately updated, the use of information from other antennas is required.

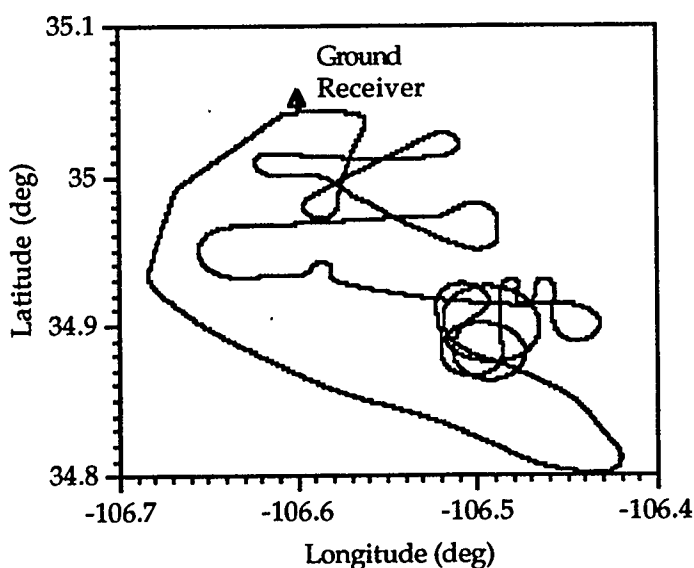
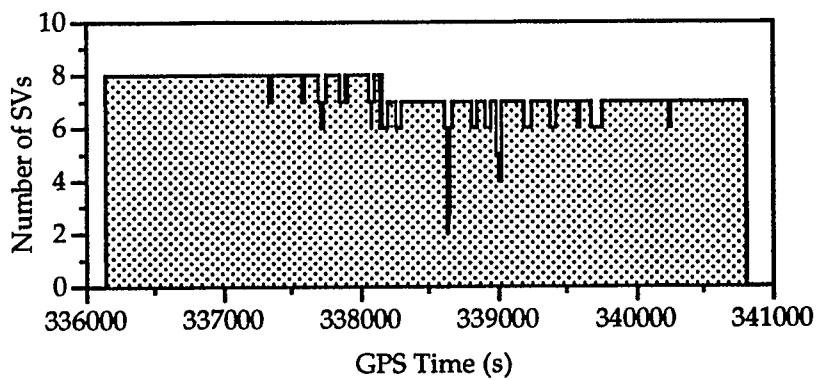
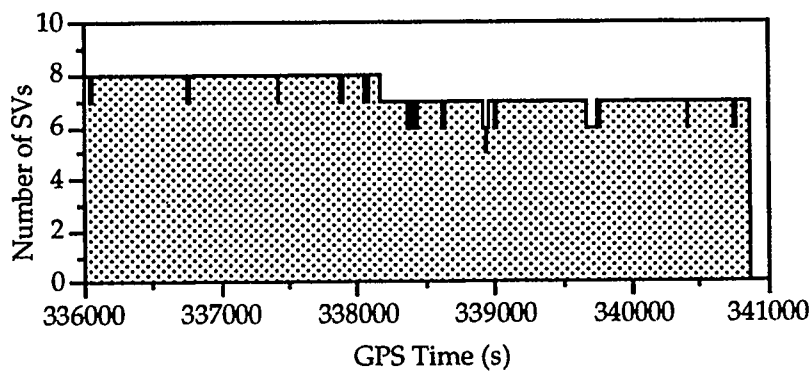


Figure 5.28
Aircraft Trajectory During the February 2 Test

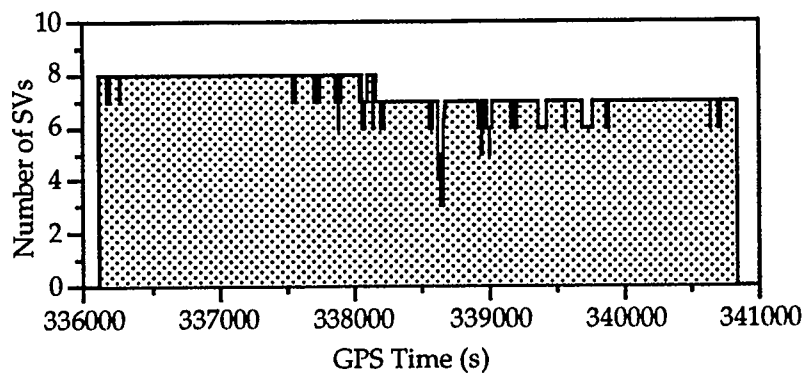
The loss of satellites is due to manoeuvres of the aircraft which can be seen from the roll and pitch of the aircraft (Figure 5.30). Maximum roll and pitch reached 60 and 30 degrees, respectively.



(a) Forward Antenna



(b) Aft Antenna



(c) Port Antenna

Figure 5.29

**Number of Satellites Observed at the Forward, Aft
and Port Antennas During the February 2 Test**

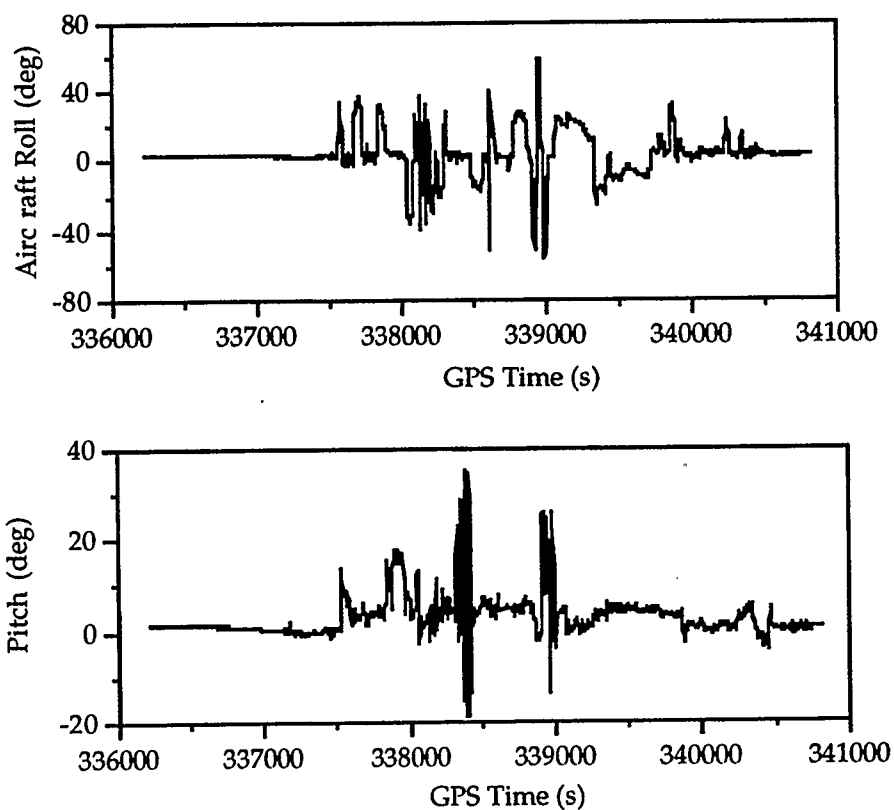


Figure 5.30
Aircraft Roll and Pitch During the February 2 Test

The integration strategy is illustrated in Figure 5.31. Before updating with the double difference carrier phase, the number of available satellites is checked. If the number of satellites is fewer than four on the first antenna, data from the next antenna is used. This procedure continues until all available pairs of double difference carrier phase are used to update the INS. In this way, the position of the IMU will be accurately maintained. This updated IMU position can be transformed to each antenna by the corresponding lever arm correction. This translated position is required to correct the carrier phase data for cycle slips or to compute the ambiguity in case a new satellite rises.

This integration system has many advantages over a conventional one antenna system, especially in airborne applications where signal shading problems occur. Only three pairs of double difference carrier phase measurements are required to keep the INS accurately updated. These measurements can either be from one antenna only or from different antennas. Carrier phase measurements from different antennas can also be used to check cycle slips or integration compatibility. The reliability of this system is greatly improved since there is no strict requirement of at least four satellites observed from one antenna. Trajectory information can be transformed from one antenna to another, so cycle slips are easier to detect and recover.

In order to analyze the effectiveness of the above method, first the GPS data from the aft antenna was processed differentially with respect to one of the ground stations using SEMIKIN™. Accurate positions of the aft antenna can be generated since there were always more than three satellites tracked at this antenna. This antenna position is transformed to the IMU using the lever arm correction of the aft antenna and the INS attitude. The resulting IMU trajectory is then treated as a reference in the following analysis.

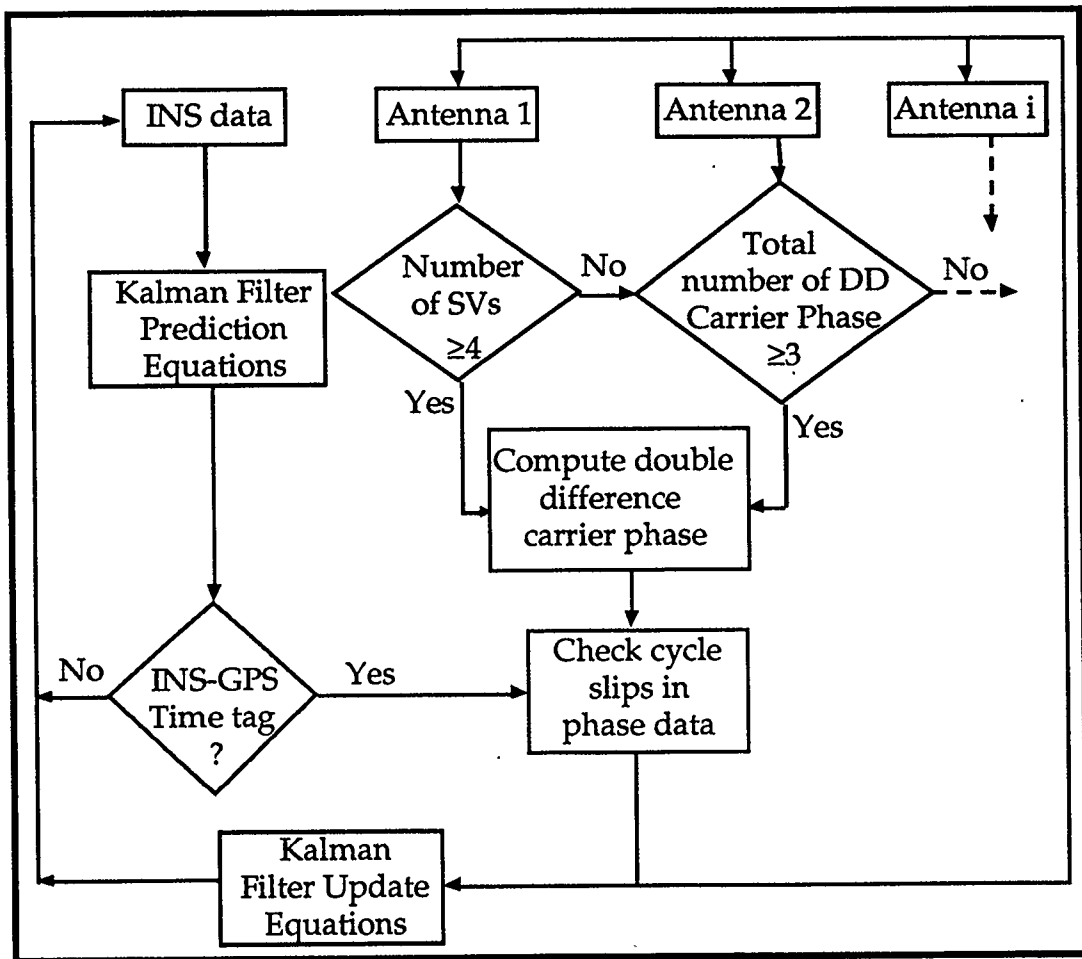


Figure 5.31

Integration Strategy of the INS with Multiple GPS Antennas

Figure 5.32 shows differences in latitude, longitude and height between the reference trajectory of the IMU and the trajectory when integrating the INS with the forward antenna only. During the period shown in the figure, the number of satellites observed is only two. Therefore a drift in the differences can be expected. The drift rate is not smooth due to the influence of the height component and the incorrect ambiguity of a new satellite observed at 338640s. The longitude differences, which are typical, between the INS without any GPS update and the reference longitude are illustrated in Figure 5.33. If the two

longitude differences are compared from Figures 5.32 and 5.33, it can be seen that the drift reaches 2.5 metres when updating with one double differenced carrier phase while the drift reaches about 3.5 metres without any update at all. Therefore, even when updating with fewer than four satellites, the INS drift rate is reduced.

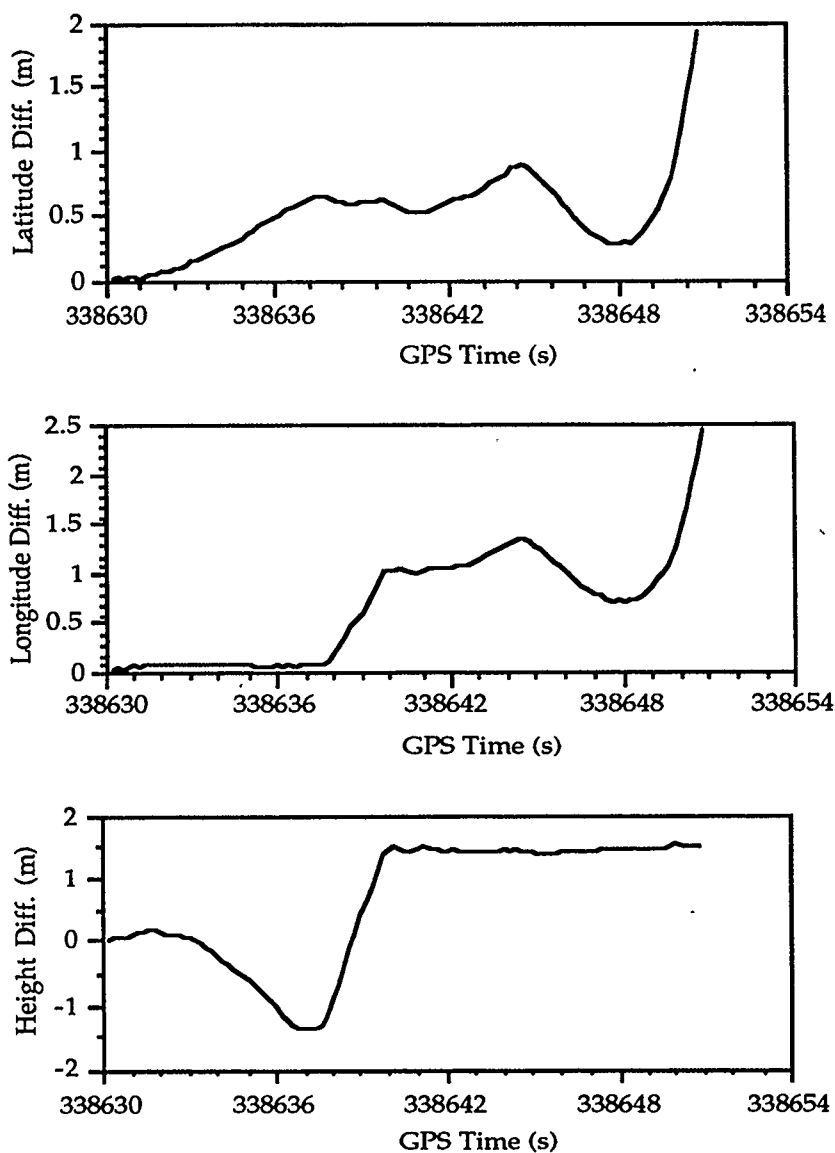


Figure 5.32
Position Differences Between the INS Integrated with
Only the Forward Antenna Only Versus the Reference Trajectory

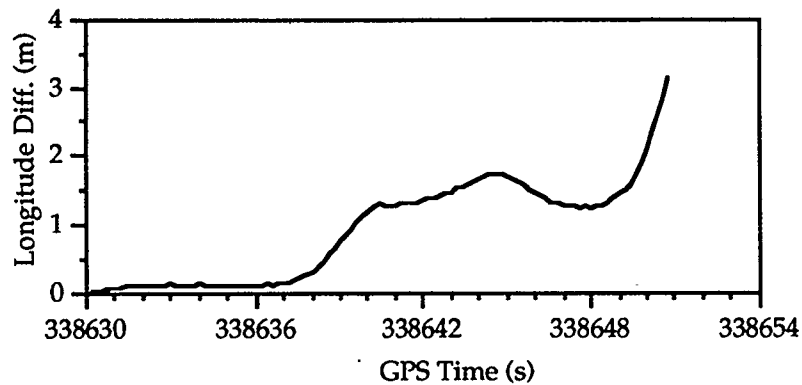


Figure 5.33
Longitude Differences Between the INS Without Update and the Reference Trajectory

If the INS is integrated with both the forward and aft antennas, the differences between the estimated position and the reference trajectory do not drift, see Figure 5.34. The RMS of the differences in latitude, longitude and height are 17, 11 and 54 mm respectively. The vibration of the differences in the latitude and longitude is due to the vibration of the barometric height which constrained the real-time filter during navigation. As can be seen, the differences in the height component reach over 10 centimetres. This is mostly due to the difficulty in modeling the barometric height.

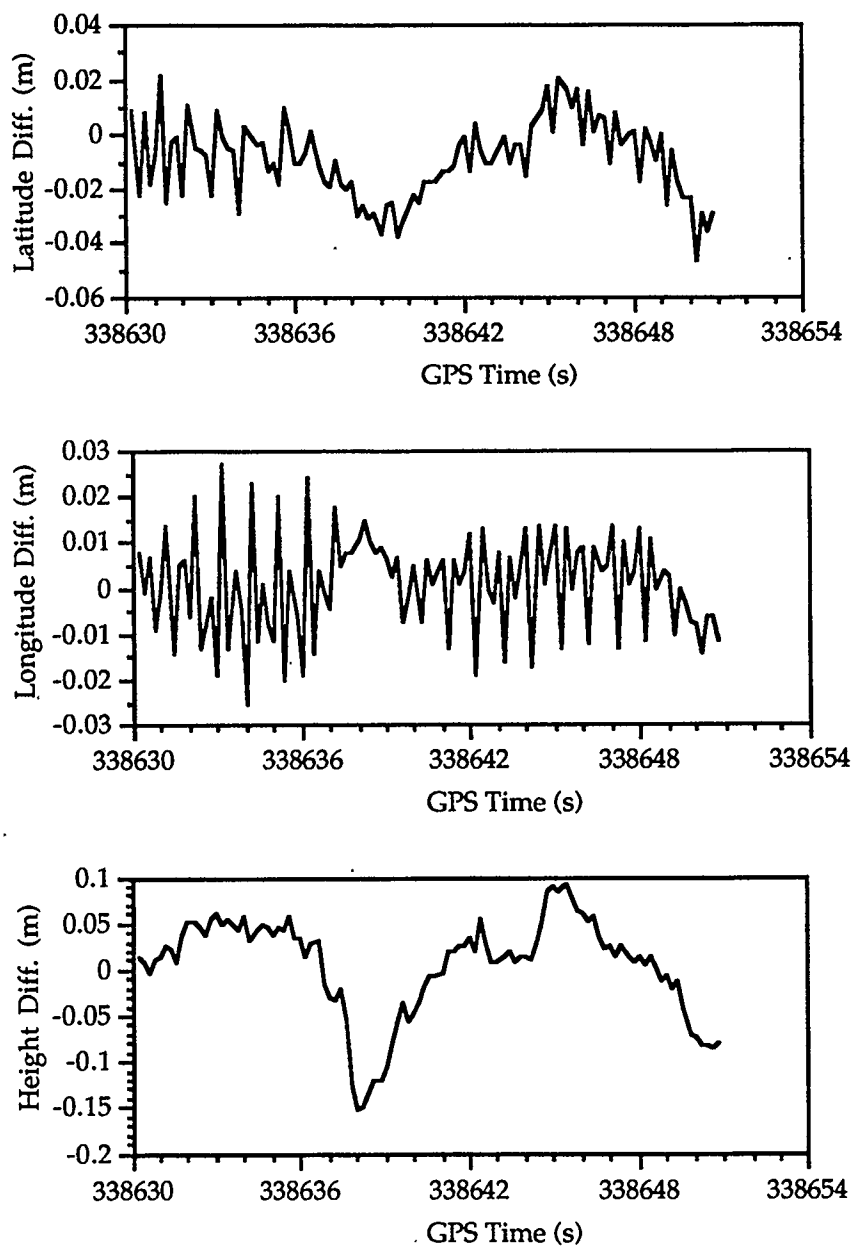


Figure 5.34
Coordinate Differences Between the INS Integrated with
the Forward and Aft Antennas Versus the Reference Trajectory

Another advantage of integrating the INS with a multi-antenna GPS system is for periods when the number of satellites at all antennas is less than four. In this case, the INS will still be accurately updated as long as there are three pairs of independent double difference carrier phase measurements available, inregardless of which antenna they are from (Sun, 1994). The test data is used to illustrate this point. Only one carrier phase measurement is used from each of the forward, aft and port antennas. They are PRNs 29-18, 29-31, 29-19 for the three antennas, respectively. Double difference carrier phase formed from PRNs 29-18 from the aft antenna is not used since it is not independent. The three measurements are integrated with the INS and then the positions of the IMU obtained in this way are compared with the reference trajectory. Figure 5.35 gives a section of these differences during the period when the aircraft was taxiing and taking off. From the figure, it can be seen that the differences are at the centimetre level. The RMS statistics are 28, 4 and 55 mm for latitude, longitude and height, respectively. These results are at the same level as when integrating the INS with the aft antenna. The lever arm effect can be seen clearly from the figure. The aircraft was taking off at about 337500s (see Figure 5.36) and the height differences also begin to climb.

Integration of multiple GPS antennas with an INS can also improve the accuracy of attitude estimation, especially of the heading component. For roll and pitch, however, the system cannot improve the accuracy significantly since the attitude accuracy from a multi-antenna GPS attitude system is not compatible with that of the INS, see Miller et al. (1993) for simulation results. Wing flexure during take-off or special manoeuvres may also significantly change the lever arms of the

antennas located on the wings which will therefore influence the roll measurements of the aircraft.

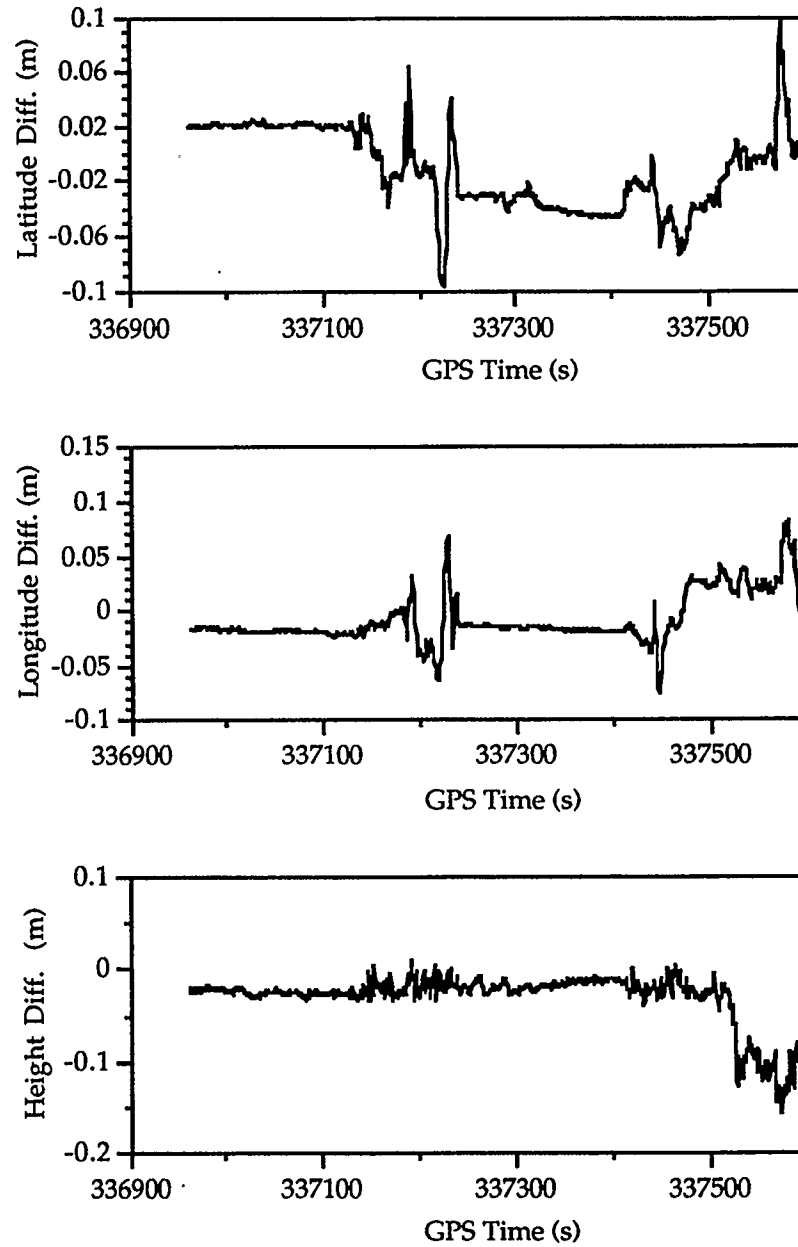


Figure 5.35
Position Differences Between the INS Integrated with Three Double
Difference Carrier Phase Measurements Versus the Reference Trajectory

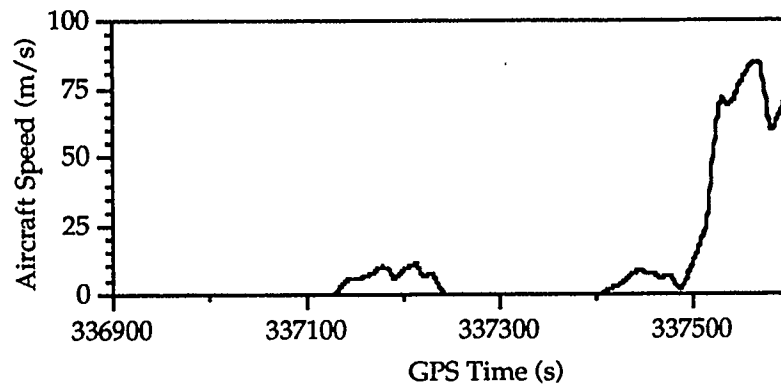


Figure 5.36
Aircraft Speed During Taxiing and Take-off
During the February 2 Test

CHAPTER 6

SUMMARY, CONCLUSIONS AND RECOMMENDATIONS

The integration of INS output position, velocity and attitude with GPS double differenced carrier phase through a centralized Kalman filter approach is investigated. Error equations of the vertical channel are derived when a barometric height is used to constrain the INS height. The capability of this GPS/INS system for precise position, velocity and attitude determination was assessed for airborne applications. GPS/INS integration software has been developed to complete this work. One potential use of the system is to determine SAR image positions using the information from the system.

A multiple day flight test and another single day flight test under different configurations, namely strapdown and gimbal configurations, are used to illustrate the methodology. Position, velocity and attitude estimated for these days are analyzed.

Attitude from a multi-antenna GPS attitude system is compared with the attitude from the INS. An aircraft wing flexure model is developed and the revised attitude results with this model are assessed.

In order to relieve the GPS signal shading problem, a strategy of integrating an INS with multiple GPS antennas is developed. Position, velocity and attitude are analyzed through a flight test where the GPS signal shading occurred. The revised results through incorporating information from other antennas are assessed. In the following, conclusions emerging from this thesis and some recommendations for further research are presented.

6.1 Conclusions

Based on the investigation done and the results obtained from the flight test data, the following conclusions can be made:

1) The attitude determined from the multi-antenna GPS attitude system used in this study is at an accuracy of 5.0, 6.6 and 3.9 arcmins for roll, pitch and heading, respectively, using antenna separations of 7 to 18 metres when modeling the aircraft wing flexure. The roll estimation accuracy is greatly improved, from 23.3 arcmins to 5.0 arcmins by using the wing flexure model. Pitch accuracy is also improved, from 7.3 to 6.6 arcmins. The amount of Twin Otter aircraft wing flexure is about 0.12 metres.

3) Differences between positions from the GPS carrier phase solution and from the GPS/INS integration solution have a RMS of about 2 cm in the horizontal components and 6 and 10 cm for height under the strapdown and the gimbal configurations, respectively. The velocity and the attitude error estimated from the GPS/INS integration are very smooth.

4) The addition of vertical channel aiding when the barometric height is used to constrain the INS height improves the height differences by reducing its RMS from 5.9 cm to 1.3 cm.

5) The utilization of multiple GPS antennas to integrate with an INS will relieve the GPS signal shading problem and improve system reliability. Position differences between the INS updated with three pairs of independent double differenced carrier phase and the reference trajectory give RMS statistics of 2.8, 0.4 and 5.5 cm for latitude, longitude and height, respectively no matter which antenna these measurements are taken from. The lever arm effect due to the aircraft wing flexure can be seen in positions from GPS/INS when information from wing antennas is used.

6.2 Recommendations

Many aspects of the current investigation need further study. They are given in the following:

1) Due to the communication speed during the data logging, only position, velocity and attitude output from the INS mechanization are used in this investigation. Raw gyro angular rates and accelerometer specific force are needed to improve the INS prediction accuracy, especially for the height prediction.

2) Velocity and attitude estimated from the GPS/INS integration have to be compared with those from external sources to evaluate the accuracy obtained from this filter.

4) A new on-the-fly ambiguity resolution method with aiding from INS is needed. The effect of the INS contribution to ambiguity resolution needs to be evaluated when GPS cannot fix the ambiguities alone.

5) In-flight alignment is needed to be analyzed for the system. The time needed to align the INS in flight when using multiple GPS antennas and the response of attitude error to aircraft dynamics needs to be studied.

REFERENCES

- Ashjaee, J. and R. Lorenz (1992), Precision GPS Surveying After Y-code, Proceedings of the Fifth International Technical Meeting of Satellite Division of ION, Albuquerque, September 16-18, pp. 657-659.
- Baustert, G., M.E. Cannon, E. Dorrer, G. Hein, H. Krauss, H. Landau, K.P. Schwarz and Ch. Schwiertz (1989), German-Canadian Experiment in Airborne INS-GPS Integration for Photogrammetric Application, Proceedings of the IAG Geodesy Symposia 102, Springer Verlag, New York.
- Bickel, D.L. and W.H. Hensley (1993), General Equation for Height Mapping in Interferometric SAR, Internal Memo of Sandia National Laboratories, Albuquerque, New Mexico.
- Blanchard, R.L. (1972), An Improvement to an Algorithm for Computing Aircraft References Altitude, IEEE Transaction on Aerospace and Electronic Systems, Vol. 8, No. 5, pp. 685-686.
- Britting, K.R. (1971), Inertial Navigation System Analysis, Wiley-Interscience, New York.
- Burgett, S. (1994), Target Location in WGS-84 Coordinates Using Synthetic Aperture Radar Images, Proceedings of IEEE Position Location and Navigation Symposia, Las Vegas, Nevada, April 11-15, pp. 57-65.

Cannon, M.E. (1987), Kinematic Positioning Using GPS Pseudorange and Carrier Phase Observations, Report No. 20019, Department of Surveying Engineering, The University of Calgary.

Cannon, M.E. (1990), High-Accuracy GPS Semikinematic Positioning: Modeling and Results, Navigation, Journal of the Institute of Navigation, Vol. 37, No. 1, pp. 53-64.

Cannon, M.E. (1991), Airborne GPS/INS with an Application to Aerotriangulation, Report No. 20040, Department of Surveying Engineering, The University of Calgary.

Cannon, M.E., H. Sun, T.E. Owen and M. Meindl (1994), Assessment of a Non-Dedicated GPS Receiver System for Precise Airborne Attitude Determination, Proceedings of the Seventh International Technical Meeting of the Satellite Division of ION, Salt Lake City, September 20-23 (in press).

Chen, D. (1993), Fast Ambiguity Search Filter (FASF): A Novel Concept for GPS Ambiguity Resolution, Proceedings of the Sixth International Technical Meeting of Satellite Division of ION, Salt Lake City, September 22-24, pp. 781-787.

Chen, D. and G. Lachapelle (1994), A Comparison of FASF and Least-Squares Search Algorithms for Ambiguity Resolution On The Fly, Proceedings of International Symposium on Kinematic Systems in Geodesy, Geomatics and Navigation, Banff, August 30-September 2 (in press).

- Cohen, C.E., B.W. Parkinson and B.D. McNally (1993), Flight Test of Attitude Determination Using GPS Compared Against an Inertial Measurement Unit, Proceedings of the ION National Technical Meeting, San Francisco, CA, January 20-22, pp. 579-587.
- Cox, D.B. (1978), Integration of GPS with Inertial Navigation System, Navigation, Journal of the Institute of Navigation, Vol. 25, No. 2, pp. 236-245.
- Diefes, D., F. Fan and C. Rodgers (1993), Dynamic GPS Attitude Determining System for Marine Application, Concept Design and Development Test Results, Proceedings of the National Technical Meeting, San Francisco, January 20-22, pp. 569-578.
- Fellerhoff, J.R. and S.M. Kohler (1992), Development of a GPS-Aided Motion Measurement, Pointing and Stabilization System for a Synthetic Aperture Radar, Proceedings of the 48th ION Annual Meeting, Washington, D.C., June 29-July 1, pp. 291-296.
- Forsberg R. (1990), Experience with the ULISS-30 Inertial Surveying System for Local Geodetic and Cadastral Network Control, Proceedings of the International Symposium on Kinematic Systems in Geodesy and Remote Sensing, Springer Verlag, New York, pp. 10-13..
- Gelb, A. (ed.) (1974), Applied Optimal Estimation, The M.I.T. Press, Cambridge, Massachusetts.
- Hartman, R.G. (1988), An Integrated GPS/IRS Design Approach, Navigation, Journal of the Institute of Navigation, Vol. 35, No. 1, pp. 121-134.

- Hatch, R. (1991), Instantaneous Ambiguity Resolution, Proceedings of the International Symposium on Kinematic Positioning for Geodesy, Surveying and Remote Sensing, Springer Verlag, New York, pp. 299-308.
- Keel, G., H. Jones and G. Lachapelle (1988), A Test of Airborne Kinematic GPS for Aerial Photography Methodology, Proceedings of Satellite Division's International Technical Meeting of the ION, Washington, D.C., pp. 147-151.
- Kleusberg, A. (1990), Separation of Inertia and Gravitation in Airborne Gravimetry with GPS, Lecture Notes in Earth Sciences, Springer-Verlag, Vol. 29, pp. 47-63.
- Lachapelle, G. and K.P. Schwarz (1989), Kinematic Applications of GPS and GPS/INS - Algorithm, Processing, Equipment Trends, Global Positioning System: An Overview, International Association of Geodesy Symposia 102, Springer Verlag, pp. 298-315.
- Lachapelle, G. , M. Casey, M. Eaton, A. Kleusberg, D.E. Wells and J. Tranquilla (1987), GPS marine Kinematic Positioning - Accuracy and Reliability, The Canadian Surveyor, Vol. 41, No. 2.
- Lachapelle, G., M.E. Cannon and G. Lu (1992), High Precision GPS Navigation with Emphasis on Carrier Phase Ambiguity Resolution, Marine Geodesy, Vol. 15, No. 4, pp. 253-269.
- Lachapelle, G., M.E. Cannon and G. Lu (1993), Ambiguity Resolution On The Fly - A Comparison of P Code and High Performance C/A Code Receiver Bulletin Geodesique, Vol. 18, No. 3, pp. 185-192.

- Lachapelle, G., H. Sun, M.E. Cannon and G. Lu (1994), Precise Aircraft-to-Aircraft Positioning Using a Multiple Receiver Configuration, The Journal of Canadian Aeronautics and Space Institute, Vol. 40, No. 2, pp. 74-78.
- Lachapelle, G., G. Lu and B. Loncarevic (1994), Precise Shipborne Attitude Determination Using Wide Antenna Spacing, Proceedings of the International Symposium on Kinematic Systems in Geodesy, Geomatics and Navigation, Banff, August 30-September 2 (in press).
- Lapucha, D. (1990), Precise GPS/INS Positioning for a Highway Inventory System, Report No. 20038, Department of Surveying Engineering, The University of Calgary.
- Lichtenegger, H. and B. Hofmann-Wellenhof (1989), GPS Data Preprocessing for Cycle-Slip Detection, Global Positioning System: An Overview, International Association of Geodesy Symposia 102, Springer Verlag, pp. 57-68.
- Liu, Z. (1992), Comparison of Statistical Methods for the Alignment of Strapdown Inertial Systems, Report No. 20047, Department of Geomatics Engineering, The University of Calgary.
- Loomis, P.V.W. and G.J. Geier (1990), Inertially Aided Lane Recapture After GPS Carrier Lock Loss, Proceedings of the International Symposium on Kinematic Positioning for Geodesy, Surveying and Remote Sensing, Springer Verlag, New York, pp. 309-318.

- Lu, G., M.E. Cannon, G. Lachapelle and P. Kielland (1993), Attitude Determination in a Survey Launch Using Multi-Antenna GPS Technologies, Proceedings of the ION National Technical Meeting, San Francisco, January 20-22, pp. 251-260.
- Mader, G. (1986), Dynamic Positioning Using GPS Carrier Phase Measurements, Manuscripta Geodaetica, Vol. 11, No. 4, pp. 272-277.
- Martell, H. (1991), Applications of Strapdown Inertial System in Curvature Detection Problems, Report No. 20043, Department of Surveying Engineering, The University of Calgary.
- Meehan, T.K. et al. (1987), ROGUE: A New High Accuracy, Digital GPS Receiver, Proceedings of the IUGG Conference, Vancouver.
- Meyer-Hilberg, J. and T. Jacob (1994), High Accuracy Navigation and Landing System Using GPS/IMU System Integration, Proceedings of IEEE PLANS'94, Las Vegas, April 11-15, 1994, pp. 298-305.
- Minkler, G. and J. Minkler (1993), Theory and Application of Kalman Filtering, Megellan Book Company, Palm Bay, Florida.
- Miller, B.L., C.A. Phillips, A.G. Evans and J.E. Bibel (1993), A Kalman Filter Implementation for a Dual-Antenna GPS Receiver and an Inertial Navigation System, Proceedings of the Sixth International Technical Meeting of the Satellite Division of ION, Salt Lake City, September 1-4, pp. 593-602.

- Owen, T.E. and R. Wardlaw (1992), Evaluating the Velocity Accuracy of an Integrated GPS/INS System: Flight Test Results, Proceeding of the ION National Technical Meeting, San Diego, January 27-29, pp. 13-22.
- Purcell, Jr., G.H., J.M. Srinivasan, L.E. Young, S.J. DiNardo, E.L. Hushbeck, Jr., T.K. Meehan, T.N. Munson and T.P. Yunck (1989), Measurement of Aircraft Position, Velocity and Attitude Using Rogue GPS Receivers, Proceedings of the Fifth International Geodetic Symposium on Satellite Positioning, Las Cruces, March 13-17.
- Schade, H., M.E. Cannon and G. Lachapelle (1993), An Accuracy Analysis of Airborne Kinematic Attitude Determination with the NAVSTAR/Global Positioning System, SPN Journal, Vol. 3, No. 2, pp. 90-95.
- Schmidt, G.T. (1978), Introduction and Overview of Strapdown Inertial System, AGARD Lecture Series No. 95; Neuilly sur Seine, France.
- Schwarz, K.P. (1983), Inertial Surveying and Geodesy, Reviews of Geophysics and Space Physics, Vol. 21, No. 4, pp. 878-890.
- Schwarz, K.P., G.S. Fraser and P.C. Gustafson (1984), Aerotriangulation without Ground Control, International Archives of Photogrammetry and Remote Sensing, 25, Part A1, Rio de Janeiro, June 16-29.
- Schwarz, K.P., M.E. Cannon and R.V.C. Wong (1989), A Comparison of GPS Kinematic Models for the Determination of Position and Velocity Along a Trajectory, Manuscripta Geodaetica, Vol. 14, No. 5, pp. 345-353.

- Schwarz, K.P., A. El-Mowafy and M. Wei (1992), Testing a GPS Attitude System in Kinematic Mode, Proceedings of the Fifth International Technical Meeting of the Satellite Division of ION, Albuquerque, September 16-18, pp. 801-809.
- Schwarz, K.P., M.A. Chapman, M.E. Cannon and P. Gong (1993), An Integrated INS/GPS Approach to the Georeferencing of Remotely Sensed Data, Photogrammetric Engineering & Remote Sensing, Vol. 59, No. 11, pp. 1667-1674.
- Siouris, G.M. (1993), Aerospace Avionic Systems, Academic Press, Inc., San Diego, California.
- Sun, H., M.E. Cannon, T. Owen and M. Meindl (1994), An Investigation of Airborne GPS/INS for High Accuracy Position and Velocity Determination, Proceedings of the ION National Technical Meeting, San Diego, January 27-29, pp. 801-809.
- Sun, H. (1994), Integration of INS with Multiple GPS Antennas, Proceedings of the Seventh International Technical Meeting of the Satellite Division of ION, Salt Lake City, September 20-23 (in press).
- Tafel, R.W., Jr. (1981), Rapid Alignment of Aircraft Strapdown Inertial Navigation System Using Navstar Global Positioning System (GPS), AGARD-CP-289, 1981.
- Tiemeyer, B., M.E. Cannon, G. Lachapelle and G. Schanzer (1994), Satellite Navigation for High Precision Aircraft Navigation with Emphasis on

Atmospheric Effects, Proceedings of IEEE PLANS'94, Las Vegas, April 11-15, 1994, pp. 394-401.

Townsend, B. and P. Fenton (1994), A Practical Approach to the Reduction of Pseudorange Multipath Errors in a L1 GPS Receiver, Proceedings of the 7th International Technical Meeting of the Satellite Division of ION, Salt Lake City, September 20-23 (in press).

Upadhyay, T.N., et al. (1982), Benefits of Integrating GPS and Inertial Navigation System, Proceedings of the ION 38th Annual Meeting, Washington, D.C., pp. 120-132.

Van Dierendonck, A.J., P. Penton and T. Ford (1992), Theory and Performance of Narrow Correlator Spacing in a GPS Receiver, Navigation, Journal of the Institute of Navigation, Vol. 39, No. 3, pp. 265-283.

Van Dierendonck, K.J., M.E. Cannon, M. Wei and K.P. Schwarz (1994), Error Sources in GPS-Determined Acceleration for Airborne Gravimetry, Proceedings of the ION National Technical Meeting, San Diego, January 24-26, pp. 811-820.

Van Graas, F. and M. Braasch (1991), GPS Interferometric Attitude and Heading Determination: Initial Flight Test Results, Navigation, Journal of the Institute of Navigation, Vol. 38, No. 4, pp. 297-316.

Wei, M. and K.P. Schwarz (1990), A Strapdown Inertial Algorithm Using an Earth-Fixed Cartesian Frame, Navigation, Journal of the Institute of Navigation, Vol. 37, No. 2, pp. 153-167.

- Wei, M. and K.P. Schwarz (1990), Testing a Decentralized Filter for GPS/INS Integration, Proceedings of IEEE Position Location and Navigation Symposia, Las Vegas, Nevada, March 20-23, pp. 429-435.
- Wei, M., S. Ferguson and K.P. Schwarz (1991), Accuracy of GPS-Derived Acceleration from Moving Platform Tests, Proceedings of IAG Symposium G3 'From Mars to Greenland: Charting Gravity with Space and Airborne Instruments', Springer-Verlag, New York, pp. 235-249.
- Wells, D.E., N. Beck, D. Delikaraoglou, A. Kleusberg, E.J. Krakiwsky, G. Lachapelle, R.B. Langley, M. Nakiboglou, K.P. Schwarz, J.M. Tranquilia and P. Vanicek (1987), Guide to GPS Positioning, Canadian GPS Associates, Fredericton, New Brunswick, Canada.
- Widnall, W.S. and P.K. Sinha (1980), Optimizing the Gains of the Baro-Inertial Vertical Channel, AIAA Journal of Guidance and Control, Vol. 3, No. 2, pp. 172-178.
- Wilson, G.J. and J.D. Tonnemacher (1992), A GPS Attitude Determination System, Marine Geodesy, Vol. 45, No. 2, pp. 192-204.
- Wong, R.V.C. and K.P. Schwarz (1983), Dynamic Positioning with an Integrated GPS-INS - Formulae and Baseline Tests, Publication 30003, Department of Surveying Engineering, The University of Calgary.
- Wong, R.V.C. (1985), A Kalman Filter-Smoother for an Inertial Survey System of Local Level Type, Report No. 20001, Department of Surveying Engineering, The University of Calgary.

Wong, R.V.C., K.P. Schwarz and M.E. Cannon (1988), High-accuracy Kinematic Positioning by GPS-INS, Navigation, Journal of the Institute of Navigation, Vol. 35, No. 2, pp. 275-287.

Wong, R.V.C. (1988), Development of a RLG Strapdown Inertial Survey System, Report No. 20027, Department of Surveying Engineering, The University of Calgary.